Nuclear and cytoplasmic huntingtin inclusions exhibit distinct biochemical composition, interactome and ultrastructural properties

Nathan Riguet[1], Anne-Laure Mahul-Mellier[1], Niran Maharjan[1], Johannes Burtscher[1], Marie Croisier[2], Graham Knott[2], Janna Hastings[1,3], Alice Patin[1], Veronika Reiterer[4], Hesso Farhan[4], Sergey Nasarov[1] and Hilal A. Lashuel[1]*

*Correspondence: hilal.lashuel@epfl.ch

Affiliations:

[1]Laboratory of Molecular and Chemical Biology of Neurodegeneration, Brain Mind Institute, Ecole Polytechnique Fédérale de Lausanne (EPFL), 1015 Lausanne, Switzerland.

[2]BIO EM facility (BIOEM), EPFL, 1015 Lausanne, Switzerland.

[3] Bioinformatics Competence Centre (BICC), EPFL, 1015 Lausanne, Switzerland.

[4]Institute of Pathophysiology, Medical University of Innsbruck, Innsbruck, Austria.

Running title:

Ultrastructure and composition of cellular Huntingtin inclusions

Keywords:

Huntington's Disease, Huntingtin, Httex1, Inclusion, Polyglutamine, Nt17, GFP, Fibrils, Electron Microscopy, 3D modeling, CLEM, Proteomics, Tomography

Abstract

Despite the strong evidence linking the aggregation of the Huntingtin protein (Htt) to the pathogenesis of Huntington's disease (HD), the mechanisms underlying Htt aggregation and neurodegeneration remain poorly understood. Herein, we investigated the ultrastructural properties and protein composition of Htt cytoplasmic and nuclear inclusions in mammalian cells and primary neurons overexpressing mutant exon1 of the Htt protein. Our findings provide novel insight into the ultrastructural properties of cytoplasmic and nuclear Htt inclusions and their mechanisms of formation. We show that Htt inclusion formation and maturation are complex processes that, although initially driven by polyQ-dependent Htt aggregation, also involve 1) polyQ and PRD domain-dependent sequestration of lipids and cytoplasmic and cytoskeletal proteins related to HD dysregulated pathways; 2) recruitment and accumulation of remodeled or dysfunctional membranous organelles, and 3) impairment of the protein quality control and degradation machinery. We also show that nuclear and cytoplasmic Htt inclusions exhibit distinct biochemical compositions and ultrastructural properties, suggesting different mechanisms of aggregation and toxicity.

Graphical Abstract

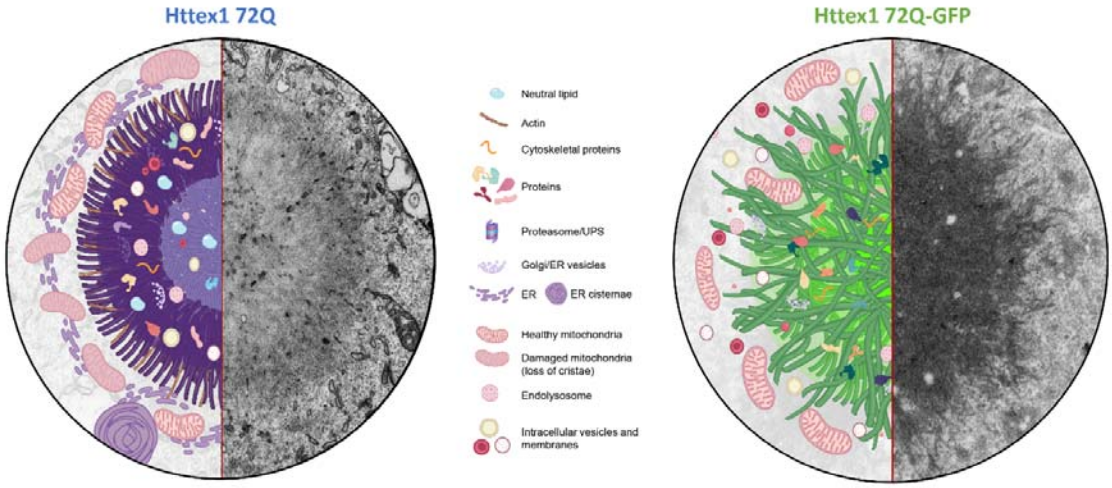

Schematic depictions and original electron micrographs of cytoplasmic inclusions formed by native (tag-free) mutant Huntingtin exon1 proteins (Httex1 72Q, left) and the corresponding GFP fusion protein (Httex1 72Q-GFP, right).

Introduction

Huntington's disease (HD) is an autosomal dominant genetic and progressive neurodegenerative disorder caused by the abnormal expansion of CAG trinucleotide repeats within exon 1 of the huntingtin gene (*HTT)*[1–4]. The expanded repeats are translated into a long pathogenic polyglutamine (polyQ) tract (>36 repeats) that renders the Huntingtin protein (Htt) more prone to aggregate[5]. The length of the CAG repeat is inversely correlated to the age of onset, with the juvenile form associated with a polyQ repeat length of 75 or more[6,7]. The accumulation of Htt-positive intraneuronal aggregates and inclusions in the cortex and the striatum of *post-mortem* brain from HD patients and in animal and cellular models of HD[2] has led to the hypothesis that Htt aggregation plays a central role in the pathogenesis of HD. However, our understanding of the ultrastructural and biochemical composition of Htt inclusions and the molecular mechanisms that drive their formation, clearance, and toxicity remains incomplete. Addressing this knowledge gap is crucial to understand the molecular and cellular mechanisms underpinning HD and to enable the development of effective therapies and disease-modifying strategies for this disease.

Although several studies have investigated specific cellular mechanisms linked to Htt aggregation, the current models often lack detailed characterization of the inclusions at both the biochemical and structural levels. Furthermore, while some of the previous studies explored the effect of polyQ repeat length on the ultrastructure properties of mutant Htt, there are no reports on the role of the first N-terminal 17 amino acids (Nt17) of Htt – which regulates many aspects of the aggregation and cellular properties of Htt proteins[8–11] – on the organization and ultrastructure properties of cytoplasmic and nuclear Htt inclusions. Finally, the vast majority of the previous studies used mutant Htt constructs fused to either peptide-based tags or large fluorescent proteins like GFP that could interfere with the cellular and aggregation properties of Htt[12–15].

Here, we employed cellular and neuronal models of Htt cytoplasmic and nuclear inclusion formation to gain insight into how sequence modifications influence the final ultrastructural and biochemical properties of cytoplasmic and nuclear Htt inclusions and their impact on cellular organelles and functions. The cellular models used in this study are based on the overexpression of N-terminal fragments of mutant Htt comprising the Exon 1 region (Httex1), which contains the polyQ expansion. Incomplete splicing of *HTT* leading to Httex1 protein expression has been shown to occur in HD patient's brains[16], and Httex1 protein was previously described as a key component of the intracellular inclusions found in HD *post-mortem* brains[16–18]. Moreover, the expression of pathogenic Httex1 (polyQ tract > 43Q) is sufficient to induce HD-like features, including aggregates formation and toxicity in mice[19–21], Drosophila[22], C. elegans[23] and cell culture models[11,12,15,24–31]. *In vitro* and cellular studies also showed that Httex1 aggregates in a polyQ repeat length and concentration-dependent manner[32–34]. Therefore the mutant Httex1-based models are useful to study the pathogenesis of HD as they reproduce different aspects of Htt aggregation and have been instrumental in advancing our understanding of the sequence, molecular, and structural determinants of Htt aggregation and inclusion formation[10,26–29,35,36].

We applied Correlative Light and Electron Microscopy (CLEM) and proteomics-based approaches to investigate the structural and biochemical properties of the cytoplasmic and nuclear Httex1 inclusions in HEK 293 cells and primary cortical neurons. We also investigated the role of the Nt17 domain and the polyQ tract length in modulating the composition and the structural and toxic properties of mutant Httex1 inclusions. Finally, given that a large body of published cellular studies on the mechanisms of Httex1 aggregation and inclusion formation is based on constructs in which Httex1 is fused to the GFP[9,11,12,37–40], we also compared, for the first time, the composition, ultrastructural properties, and toxicity of inclusions formed by native (tag-free) and GFP-tagged mutant Httex1.

Our results demonstrate that Htt inclusions are composed of a complex mixture of aggregated mutant Httex1, different cellular proteins, and membranous organelles, including

the endosomal system. We show that functional and ultrastructural properties of Httex1 inclusions are differentially altered by sequence modifications and interactions with lipids and cellular organelles. We demonstrate that Htt cytoplasmic and nuclear inclusions exhibit distinct composition and ultrastructural properties, suggesting different mechanisms of aggregation, inclusion formation and toxicity. These observations revealed that the differences in the cellular environment and interactome could influence the mechanisms of aggregation, the structural and biochemical properties of the inclusions, and their relative contribution to mutant Htt-induced toxicity. Finally, we show that inclusions produced by mutant Httex1 72Q-GFP exhibit striking differences in terms of organization, ultrastructural properties, protein composition, and their impact on mitochondrial functions compared to the inclusions formed by the tag-free mutant Httex1 72Q. Overall, our findings contribute to a better understanding of the sequence, molecular, and cellular determinants of mutant Httex1 aggregation, inclusion formation and toxicity. They also underscore the critical importance of further studies to investigate the role that lipids, organelles, and the Htt interactome play in Htt pathology formation and maturation and Htt-induced toxicity in HD.

Results

Httex1 cytoplasmic inclusions exhibit a distinctive core and shell morphology and are composed of highly organized fibrils, cytoplasmic proteins and membranous structures

To investigate the ultrastructural properties of Htt inclusions, we first used a mammalian cell model system of HD, in which overexpression of mutant Httex1 with polyQ repeats > 39 has been shown to result in a robust and reproducible formation of cytoplasmic Htt inclusions[15,29]. In this model, nuclear inclusions are also observed in ~ 15% of transfected cells by Httex1 72Q[41], thus providing an opportunity to investigate and compare the ultrastructural features of cytoplasmic and nuclear Htt inclusions under identical conditions. This model system is widely used to investigate molecular, cellular, and pharmacological modulators of Htt aggregation and inclusion formation[11,12,15,24–31,42,43], though very often using Htt constructs with extra non-natural sequences such as Myc, FLAG and GFP tags. Previous studies have shown that the presence of such tags significantly alters the aggregation properties of N-terminal fragments of mutant Htt[44–46]. Therefore, in this work, we opted to maintain the native sequence of the protein and investigated mutant Httex1 aggregation and inclusion formation in the absence of additional sequences or tags. Tag-free Httex1 72Q was overexpressed in HEK 293 cells (HEK cells), and the morphology and structural properties of Httex1 inclusions were assessed. Despite the formation and abundance of inclusions formed by Httex1 72Q, we did not observe overt toxicity in HEK cells. The initiation of apoptotic events was apparent only after 96 h, as indicated by Caspase 3 activation without loss of plasma membrane integrity[41].

Next, we assessed the morphology of Httex1 72Q inclusions by immunocytochemistry (ICC) using nine antibodies against different epitopes along the sequence of Httex1 (Figures 1A and S1). Interestingly, all the antibodies presented a strong immunoreactivity to the periphery of the Httex1 72Q inclusions, and none of these antibodies labeled the core of these inclusions (Figures 1B and S2A). This observation suggests either an absence of Htt in the center of the inclusions or poor accessibility of the used antibodies to the core of the

inclusions, possibly due to the high compactness of the Htt aggregates in the core compared to the periphery of the inclusions. In addition, we observed high colocalization of the filamentous actin (visualized by phalloidin) with Httex1 inclusions (Figure 1B, white arrowheads), indicating a possible involvement of the cytoskeleton proteins in Htt inclusion formation.

To gain more insight into the structural and organizational features of Httex1 inclusions formed in cells, we turned to electron microscopy (EM). We first employed a correlative approach to analyze the ultrastructure of the inclusions by EM and their subcellular environment seen with CLEM (Figure 1C-D). Httex1 72Q positive inclusions were immunostained and imaged by confocal microscopy (Figure 1C) and then subjected to serial sectioning for analysis by EM (Figure 1D). The EM micrographs of the Httex1 72Q inclusions revealed a surprisingly complex morphology characterized by a halo-like structure with a dense core and a heavily stained outer shell. The outer layer of the inclusions contained fibrillar structures that appeared to be tightly packed and radiating from the core of the inclusion. EM-dense cytoplasmic structures were detected in both the core and the periphery and could reflect the incorporation or sequestration of disrupted organelles inside the inclusion[12,47,48] (Figure 1D, white arrowheads). The halo-morphology of Httex1 inclusions was consistent across many imaged inclusions (Figure S3A).

To further characterize the structural properties and distribution of Httex1 within the inclusion, we used cryo fixation via high-pressure freezing, which preserves the cellular ultrastructure in its native state. EM imaging revealed radiating fibrils at the periphery and more tightly organized and stacked fibrils in the core (Figure S4A). Electron-dense membranous structures were observed in the core and more to the periphery. These results suggest that both the core and shell contain aggregated fibrillar forms of mutant Htt but with a distinct structural organization. The structural organization of Httex1 72Q inclusions combined with the primary localization of Htt antibodies in their periphery suggests that Htt fibrils in the outer layer of these inclusions serve as active sites for the recruitment of soluble Htt, the growth of Htt fibrils, and the interaction of Htt with other proteins and cellular organelles. The

ultrastructure of inclusions formed by the Httex1 72Q suggests that their formation is not simply the result of the interactions between Htt monomers but may also involve interactions and the recruitment of other proteins and cellular components.

To determine whether the formation of cytoplasmic inclusions involves interactions with or recruitment of membranous structures such as ER and mitochondria, we imaged inclusion positive cells by EM under conditions that preserve the internal membranes of cellular organelles, i.e., in the absence of detergents commonly used in the ICC procedure. EM images revealed that the core and periphery of the Httex1 72Q inclusion contained many small membranous structures (Figure 1E, yellow arrowheads). An ER network and mitochondria were present at the periphery of these inclusions, suggesting that these regions might act as active sites for the recruitment and interaction of soluble Htt with other proteins and cellular compartments during inclusion formation and maturation. Most of the mitochondria surrounding the cytoplasmic Httex1 72Q inclusions exhibited damaged or markedly reduced numbers of cristae (Figure 1E, green arrowheads). We next generated a 3D model of the inclusions and the organelles in their vicinity (Figure 1E-F). The 3D model confirmed that inclusions are formed in a crowded region with ER and mitochondria all around it. The 3D also model suggested that the electron-dense membranous structures recruited inside the Httex1 inclusions were mostly composed of endomembranes and vesicles (labeled in white), consistent with a previous report[12,47]. Interestingly, the ER adopted a specific “rosette-like” or “stacked cisternae” morphology (highlighted by a red arrowhead) in the periphery of some Httex1 72Q inclusions. Finally, it is noteworthy that the mitochondria (labeled in yellow, Figure 1F) were not detected inside the inclusion but rather at the periphery of the inclusions. Interestingly, despite their proximity to the nucleus, the inclusion did not compromise the nuclear membrane integrity (Figure S3A).

Next, we sought to identify the endomembrane compartments within Httex1 72Q inclusions using a panel of antibodies or dyes labelling intracellular compartments. The mitochondrial (Tom 20 and Mitotracker) and ER (BiP/Grp78) markers were strongly detected near Httex1

72Q cytoplasmic inclusions (Figure S5A-C). The autophagy flux marker, p62, was enriched in the periphery of Httex1 72Q inclusions (Figure S5D). Markers of aggresome formation, such as Vimentin and HDAC6, were also enriched in the periphery and in close proximity to Httex1 72Q inclusions (Figure S5E-F). Moreover, when cytoskeletal proteins such as actin and tubulin were overexpressed (fused with RFP), they were observed mainly at the periphery of the Httex1 72Q inclusions (Figure S5G-H). This observation is consistent with the colocalization of F-actin (stained by phalloidin) with Httex1-72Q inclusions (Figure 1B, white arrowheads). None of the organelles' markers were detected inside the core of these inclusions (Figure S5), although the EM images clearly showed the presence of membranous structures in the center (Figure 1E). This confirms the poor accessibility of antibodies and dyes to stain the core of the Httex1 inclusions likely due to their compactness and highlights the importance of using EM to decipher the ultrastructural properties and composition of the pathological inclusions.

Altogether our data suggest that Httex1 aggregates could form at the surface of membranes as suggested by Suoponki and colleagues[49], which could promote early aggregation events as well as membrane perturbation and their recruitment into cytoplasmic Httex1 inclusions.

Cytoplasmic and nuclear Httex1 inclusions in HEK cells exhibit distinct ultrastructural properties

Both cytoplasmic and nuclear inclusions have been observed in HD patients' brains and transgenic mouse models of HD[50–52]. Therefore, we compared the structural and organizational properties of Httex1 72Q inclusions in the cytoplasm (~85%) and nucleus (~15%) of the transfected HEK cells containing inclusions[41]. Using immunofluorescence-based confocal microscopy, we did not observe significant differences in the size or overall morphology between the Httex1 72Q inclusions in the nucleus and the perinuclear region (Figure 2A). However, EM clearly showed that the nuclear inclusions formed by the Httex1 72Q were enriched in fibrillar structures (Figure 2B) but did not exhibit the classical core and

shell organization nor did they contain the membranous structures trapped within the cytoplasmic inclusion (Figure 1D-E). This suggests that the intracellular environment is a key determinant of the structural and molecular complexity of the inclusions and that nuclear and cytoplasmic inclusion formation occurs via different mechanisms.

The length of the polyQ domain is another key determinant of inclusion formation

We and others have previously shown that the polyQ repeat length strongly influences the conformation and aggregation properties of Httex1, with higher polyQ favoring the formation of a more compact polyQ domain and accelerating Htt aggregation *in vitro* and *in vivo*[34,45,53]. However, the polyQ dependence on Htt inclusion formation has predominantly been assessed mainly by ICC and in the context of Htt fused to fluorescent proteins and polyQ repeats much longer than the pathogenic threshold (64Q-97Q[12]; 64Q-150Q[30]; 43Q-97Q[14]). Therefore, we next investigated whether the length of the polyQ repeat also influences the organization and ultrastructural properties of cytoplasmic Htt inclusions in HEK cells. Toward this goal, we investigated the level of aggregation and the structural organization of the Httex1 inclusions carrying different polyQ lengths (16Q, 39Q vs. 72Q). Consistent with previous data from our group, no significant cell death was observed in HEK cells overexpressing Httex1 16Q or 39Q constructs even after 96 h[41]. However, cells expressing Httex1 72Q underwent apoptosis after 96 h. As expected, no inclusions were formed upon overexpression of Httex1 16Q even after 72 h post-transfection (Figure S6). Httex1 39Q inclusions were detected predominantly in the cytoplasm of the HEK cells at all the time points examined (24-72 h), though at lower numbers than in the Httex1 72Q conditions: Httex1 39Q (16%) vs. Httex1 72Q (38%) of transfected cells[41].

The dark shell structure that delimits the core from the periphery of the Httex1 72Q inclusions (Figure 1D-E) was absent in the Httex1 39Q inclusions (Figure 1G). In addition, the Httex1 39Q inclusions appeared less dense compared to those of the Httex1 72Q. These observations were consistent for all eight inclusions imaged per condition (Figure S3B).

Similar to what we observed for Httex1 72Q, the 3D reconstruction of the Httex1 39Q inclusions clearly showed alteration of the ER organization, as well as the localization of mitochondria near the inclusions (Figure 1H). The electron-dense membranous structures found inside the inclusions were identified as endomembranes and vesicles. Httex1 39Q expressing cells also contained specific ER-cisternae at the periphery of the inclusions (Figure 1H, red arrowheads). Altogether, our data establish that polyQ expansion plays a critical role in determining the final architecture and ultrastructural properties of the Httex1 inclusions.

Removal of the Nt17 domain reduces aggregation formation but does not influence the organization and ultrastructural properties of the inclusions

The Nt17 domain functions as a Nuclear Export Signal (NES) and has been shown to play an important role in regulating the intracellular localization of Htt as well as its kinetics of aggregation and extent of inclusion formation[36,54]. Therefore, we sought to assess the role of Nt17 in regulating the ultrastructural properties of Htt inclusions. Towards this goal, we generated Httex1 39Q and 72Q mutants lacking the entire Nt17 domain (ΔNt17) and compared the structural properties of the inclusions formed by these mutants to those formed by Httex1 39Q and Httex1 72Q. Quantitative confocal microscopy revealed a strong reduction in the number of inclusions (~50% reduction) of cells transfected by Httex1 ΔNt17 72Q compared to Httex1 72Q[41]. Surprisingly, inclusions formed by the Httex1 ΔNt17 72Q (Figure S7A-B) exhibited an architecture and organization (central core and peripheral shell) similar to those formed by Httex1 72Q (Figure 1D-E and Figure S8A). Furthermore, similar to Httex1 39Q, the Httex1 ΔNt17 39Q cytoplasmic inclusions did not exhibit a core and shell architecture. These observations suggest that the Nt17 domain – while playing a crucial role in regulating the kinetics and early events of Htt aggregation – does not influence the morphology or structural organization of Htt cytoplasmic and nuclear inclusions. This is surprising given that *in vitro* and cellular studies have consistently shown that the Nt17 domain plays an important role in regulating the kinetics and structural properties of Htt

aggregation[11,41] and Htt interactions with lipids and membranes[8,9,55–57]. In a recent study using solid-state nuclear magnetic resonance spectroscopy (ssNMR), Boatz *et al.* showed that the Nt17 domain and part of the PRD (PPII helices) are buried in the core of the fibrils, while the other part of the PRD (random coil) remains dynamic, accessible and regulates multifilament assemblies *in vitro*[58]. Together, these observations could explain why the deletion of the Nt17 domain does not interfere with the organization of the inclusion and suggest that the interactions between the fibrils and other proteins and/or organelles are most likely mediated by the flexible PRD domain.

Neutral lipids are incorporated into Httex1 cellular inclusions in a polyQ length-dependent manner

Although several studies have shown dysfunction of cholesterol metabolism in various cellular and animal models of HD[59,60], the role of lipids in Htt inclusion formation and the lipid composition of cellular huntingtin inclusions remains unknown[61,62]. To gain further insight into the role of lipids in the formation and structural organization of Httex1 inclusions, we next assessed their presence using fluorescent probes targeting different lipid classes. We did not observe the recruitment of ceramide, cholesteryl ester, or phospholipids into mutant Httex1 inclusions (Figure S9 A-C). Interestingly, neutral lipids were not found in the center of Httex1 39Q inclusions (Figure S9D white arrowheads) but were enriched in Httex1 72Q inclusions (Figure S9E). This could contribute to the polyQ length-dependent differences in the ultrastructural properties of the Httex1 inclusions (Figures 1E and 1G). Neutral lipids were also detected in nuclear inclusions (Figure S9E, yellow arrowheads). Although the Nt17 domain has been shown to act as a lipid- and membrane-binding domain, neutral lipids were also detected in the Httex1 ΔNt17 72Q inclusions, though not inside Httex1 ΔNt17 39Q inclusions (Figure S10A). These results demonstrate that polyQ-dependent interaction between Htt and neutral lipids plays an important role in Httex1 aggregation and the formation of both nuclear and cytoplasmic inclusions. Interestingly, these interactions are not dependent on the Nt17 domain, which has been reported to interact with membranes and

phospholipids. Whether mutant Httex1 interactions with lipids occur prior to aggregation and help initiate its oligomerization or represent late events associated with the maturation of inclusions remains unknown.

Quantitative proteomics reveals that the formation of Httex1 72Q inclusions involves the active recruitment and sequestration of proteins and organelles

To gain further insight into the biochemical composition of Htt inclusions, we performed quantitative proteomic analysis and compared the differentially abundant proteins between the Urea soluble fractions of HEK cells overexpressing Httex1 72Q or Httex1 16Q (see experimental details, Figure S11A-C). Western Blot analysis of the Urea fraction confirmed the presence of Httex1 72Q within inclusions, while non-pathogenic Httex1 16Q was only detected in the soluble fraction (Figure S11A).

As expected, no proteins were significantly enriched in the insoluble fraction of HEK cells expressing Httex1 16Q compared to those expressing GFP (Figure S11D). In contrast, 377 proteins were significantly enriched in the insoluble fraction of HEK cells overexpressing Httex1 72Q compared to cells overexpressing Httex1 16Q (Figure 3A). Among these proteins, we identified the endogenous HTT protein (Figure S11E). This suggests that the aggregation process triggered by the overexpression of Httex1 also leads to the recruitment of endogenous HTT protein.

Classification by cellular component (CC, Figure 3B) using the Gene Ontology (GO) showed that 55% of the proteins enriched in the insoluble fractions of HEK cells containing Httex1 72Q inclusions were part of the cytoplasmic compartment, with 24% of these proteins belonging to the endomembrane system, including the endolysosomal apparatus (clathrin-coated endocytotic vesicles, early endosome, endosomes, recycling endosomes, exosomes, and autophagosomes), the vesicles involved in Golgi-ER transport, and membranes from the Golgi and trans-Golgi network. These data are in line with the EM data showing that the Httex1 72Q inclusions were composed of small membranous structures and vesicles.

Approximately 14% of the proteins enriched in the insoluble fraction were classified as pertaining to the cytoskeleton compartment, with the actin cytoskeleton being the most predominant, consistent with our confocal results (Figure 1B). The absence of mitochondrial proteins in the soluble Urea fraction confirms that mitochondria are not sequestered inside the inclusions but, rather, accumulate at the periphery, as shown by our EM imaging. The rest of the cytoplasmic proteins sequestered in the insoluble fraction of the Httex1 72Q-transfected HEK cells were mainly from the perinuclear region or from macromolecular protein complexes such as the ubiquitin-proteasome system (UPS), the mRNA processing bodies, and the stress granules. Interestingly, the insoluble fraction of the Httex1 72Q-transfected HEK cells was also significantly enriched by proteins of the nuclear compartment (~ 45%). Among the nuclear proteins, ~ 71.6% belonged to the nucleoplasm. Proteins from the nucleolus, the nuclear bodies, the nuclear envelope, and the nuclear pore were also significantly enriched.

Classification of the enriched proteins by biological function showed that the most highly enriched terms for the GO biological process (Figure 3C) and the signaling pathways using the Ingenuity Pathway Analysis (Figure S12) were related to the proteins involved in the proteasomal ubiquitin-dependent protein degradation. Proteins from the UPS system[63], including ubiquitin moiety, E3 ubiquitin ligases (e.g., ITCH, RNF34, TRIM32), 26S proteasome subunits, and deubiquitinases formed the major cluster of the differentially enriched proteins in the Httex1 72Q inclusions. These results are in line with previous studies showing that Htt inclusions formed in HD patients or several cellular and *in vivo* models sequester several key components of the UPS system, including 26S proteasomes[64] (ADRM1[65]), deubiquitinases[66] (e.g., NEDD4 and USP5), and E3 ubiquitin ligases (e.g., ITCH, TRAF6, UBE3A, UHRF2, and Parkin) and induce impairment of the UPS[67–69]. In addition, our analysis revealed that among the proteins significantly up- or down-regulated in Httex1 72Q compared to Httex1 16Q, 42 proteins are known Htt interactors linked to the UPS, identified from the HDinHD dabase (Table S1).

Proteins involved in autophagosome formation (optineurin[70]), maturation (ubiquilins[71]), and the process of autophagosome-lysosome fusion[72] (TOLLIP-interacting proteins and proteins involved in endolysosomal trafficking) were also enriched inside the Httex1 72Q inclusions. Both TOLLIP[73–75] and optineurin[76–79] are critical for the efficient clearance of polyQ protein aggregates[80] and, in particular, for the degradation of Htt aggregates. The depletion of TOLLIP in HeLa cells increases GFP-Htt-103Q-induced toxicity[73], while optineurin knockdown promotes Htt aggregation.

In addition, several chaperones from the Hsp70 and the DnaJ/HSp40 families (e.g., DNAJB6, DNAJB2, and other proteins from the Hsp40 and Hsp70 families), as well as ubiquilin-2, found previously enriched in Htt inclusions[30,81,82], were also enriched inside the Httex1 72Q inclusions. This cluster of proteins was associated with the BAG2 signaling pathway (Figure S12), one of the top canonical signaling pathways that regulate the interplay between the chaperones from the Hsp70/Hsc70 family and ubiquitin. Interestingly, it has recently been shown that the Hsp70 complex, together with the Hsp40/110 chaperone family, formed a disaggregase complex that can directly bind to Htt aggregates[83]. After disaggregation, Ubiquilin-2 interacts with Htt and shuttles the disaggregated species to the proteasome to promote its complete degradation[84]. The enrichment of the disaggregase chaperones network in the Httex1 72Q inclusions suggests that they were actively recruited but failed in their attempt to clear the Httex1 72Q aggregates. Our proteomic analysis also revealed the enrichment of several biological processes and signaling pathways related to RNA binding proteins, transcription factors, RNA splicing, mRNA processing, and stability, as well as chromatin and nucleotide-binding proteins (Figure 3C and Figure S12). Dysregulation of transcriptional gene pathways has been reported in several animal and cell HD models[85–87] as well as in HD post-mortem tissues and HD peripheral blood cells[88–90].

Together, our proteomic and CLEM data provide strong evidence that the formation of the Httex1 72Q inclusion formation involves the active recruitment and sequestration of cellular proteins, lipids, and organelles. This also suggests that sequestration of the key transcription

regulators and depletion of key proteins from the autophagolysosomal, UPS, and chaperone pathways, due to their sequestration inside the Httex1 pathological inclusions, are major contributors to cellular dysfunction and neurodegeneration in HD of the degradation and quality control machinery, as reported in HD human brain tissue[91].

Httex1 72Q cytoplasmic inclusion formation induces mitochondrial fragmentation, increases mitochondrial respiration and leads to ER-exit site remodeling

The remarkable accumulation of damaged mitochondria at the periphery of Httex1 72Q inclusions prompted us to investigate how Htt inclusion formation impacts mitochondrial functions. Quantification of mitochondrial length from EM-micrographs revealed a shorter mitochondrial profile associated with Httex1 72Q inclusions, as compared to HEK cells transfected with empty vector (Figure 4A-B). Similar levels of the outer mitochondrial membrane protein VDAC1 suggest that this mitochondrial fragmentation was not associated with a decrease in mitochondrial density (Figure S13A). We hypothesized that the fragmentation and recruitment of mitochondria to Httex1 inclusions might be associated with respirational dysfunction. Therefore, we performed high-resolution respirometry on cells transfected with Httex1 16Q and 72Q for 48 h. Aggregates were only detected in mutant Httex1 72Q transfected cells (Figure S13B). We assessed different respirational states of mitochondria by high resolution respirometry (Figure S13C-D). Httex1 72Q transfection resulted in significantly higher mitochondrial respiration than Httex1 16Q (Figure S4C). Together, our results demonstrate a clear impact of Httex1 72Q inclusion formation on mitochondrial morphology and function.

Our EM analysis and 3D reconstruction further revealed the presence of ER cisternae at the periphery of the Httex1 inclusions. Stacked ER cisternae are usually formed by an increasing concentration of specific resident proteins or stress conditions[92]. The changes we observed in ER organization, together with the enrichment of proteins related to ER-Golgi trafficking

inside the inclusions, prompted us to investigate whether ER functions were impaired upon the formation of the Httex1 inclusions.

A major function of the ER is the biogenesis of COPII carriers that ferry proteins and lipids to distal compartments. COPII carriers form at ER exit sites (ERES), which are ribosome-free domains of the rough ER. To determine whether the formation of Httex1 inclusions interferes with the homeostasis of the ERES, we used confocal imaging and quantified the number of ERES, labelled specifically by the COPII component Sec13 protein in HeLa cells expressing Httex1 72Q, Httex1 39Q, or Httex1 16Q (Figure 4D). Our data show that the number of ERES was significantly reduced (~ 20%) only in cells containing Httex1 72Q inclusions (Figure 4E, upper panel). We next quantified the size of the ERES using the same imaging pipeline (Figure 4E, lower panel). Overexpression of Httex1 16Q caused a 20% reduction in the size of the ERES compared to EV. However, the reduction became much more significant in the cells carrying Httex1 39Q or Httex1 72Q, with a ~40% decrease compared to empty vector and ~20% compared to Httex1 16Q. These results demonstrate that the formation of the Httex1 inclusions interferes with the formation and fusion of ERES. The remodeling of ERES in cells has been described primarily as an adaptive response to the protein synthesis level of ER with the number of ERES proportional to the cargo load. Interestingly, our proteomics results (Figure 3A) showed that the TGF (Transforming Growth Factor) protein—which plays a central role in the biogenesis and organization of ERES—is sequestered in mutant Httex1 inclusions[93]. In line with our results, it has been previously shown that the depletion of TGF induced a dramatic reduction of the ERES sites[94]. Alternatively, the reduction of the ERES sites could represent early signs of cell vulnerability and toxicity induced by the presence of the Httex1 inclusions in cells.

Expression of Httex1 72Q in primary cortical neurons leads to the formation of dense and filamentous nuclear inclusions

We next investigated the sequence determinants of Htt aggregation and inclusion formation in primary cortical neurons over time. As expected, none of the Httex1 16Q constructs (Httex1 16Q and ΔNt17 Httex1 16Q) overexpressed in neurons induced the formation of aggregates up to 14 days post-transduction (D14). Conversely, overexpression of Httex1 72Q induced the formation of round nuclear inclusions in almost 100% of transduced neurons, already at D3 (Figures 5A-B and S14). Less than 1% of the neurons showed cytoplasmic inclusions, either as puncta or with the ring-like morphology. Although no changes in the subcellular distribution of the inclusions were observed up to D14, we observed significant changes in the size and shape of the nuclear inclusions over time (Figure 5C). At D3, the majority of the nuclear inclusions were detected as small (< 1 μm) nuclear puncta (94%), and only a few appeared as large (~ 3-4 μm) inclusions (Figure 5D). The ratio of small and large nuclear inclusions shifted slightly over time from 50:50 at D7 to 43:57 at D14 (Figure 5D).

We next characterized the ultrastructural properties of the nuclear Httex1 72Q inclusions by CLEM. At D7, these inclusions appeared as dense and roughly round aggregates without distinctive core and shell structural organization (Figures 6A and S15A). In these thin sections, the intranuclear Httex1 72Q inclusions appeared darker than the surrounding nucleoplasm and structurally different from the nucleolus (Figure 6A and controls Figure S15C-D). The high density of these aggregates made it challenging to determine if they were made of filamentous structures. However, using electron tomography (ET), we were able to visualize and confirm the presence of filamentous structures inside these nuclear inclusions (Figure 6B). The segmented filaments did not appear to be closely stacked in parallel but rather organized as a network of tortuous filaments. Neither EM nor ET imaging revealed the presence of membranous-, organelle- or vesicle-like structures inside or at the periphery of these inclusions. Although removal of the Nt17 domain (Figure 6C) did not alter the ultrastructural properties or composition of the inclusions, it accelerated the formation of large aggregates significantly. As early as D3, ~60% of the neurons overexpressing ΔNt17 Httex1 72Q already contained large nuclear inclusions, compared to only ~6% for Httex1

72Q (Figure 5D). At D14, almost all the aggregates formed in the ΔNt17 Httex1 72Q overexpressing neurons converted into the large nuclear inclusions (~90%) (Figure 5D), compared to 57% for Httex1 72Q.

Finally, among the small aggregates dispersed throughout the nucleus, a few were observed near the nuclear membrane, which often appeared damaged and ruptured (Figures S15A). Our data are in line with previous EM studies from human HD patients[95] and HD mice models[19,96] showing nuclear ultrastructural changes, including altered nuclear membrane shape, nuclear invagination and increased nuclear pore density in neurons bearing Httex1 inclusions. Consistent with these observations, the nuclei containing Httex1 72Q inclusions showed enhanced nuclear condensation over time (Figure 5E), indicating increased neuronal toxicity, consistent with previous reports in HD patients[97] and HD mice model[96]. Interestingly, despite the presence of the large inclusions as early as D3 in the neurons overexpressing ΔNt17 Httex1 72Q, we did not observe an earlier onset of cell death or a higher level of toxicity over time in these neurons compared to those overexpressing Httex1 72Q (Figure 5E). This suggests a lack of correlation between cell death level and the size of the inclusions, with the large inclusions being less toxic.

These results demonstrate the formation of condensed mutant Httex1 fibrillar aggregates within intranuclear inclusions in neurons and suggest that the process of their formation and maturation is directly linked to neuronal dysfunctions and cell death.

The addition of GFP to the C-terminal part of Httex1 induces a differential structural organization and toxic properties of Httex1 inclusions

Given that the great majority of cellular models of HD rely on the use of fluorescently tagged Htt constructs, we next investigated the aggregation properties of mutant Httex1 fused to GFP (Httex1 72Q-GFP and Httex1 39Q-GFP). First, we assessed the morphology of Httex1 72Q-GFP cytoplasmic inclusions in HEK cells by immunocytochemistry (ICC) using a panel

of Httex1 antibodies (Figures 7A-B and S16A). Confocal imaging revealed a diffuse GFP signal throughout the inclusions. Conversely, the Htt antibodies labeled mainly the outermost region of Httex1 72Q-GFP inclusions, but also faintly stained their centers (Figure 7B). In contrast, the tag-free inclusions' cores were not labeled by all the Htt antibodies tested. Thus, we hypothesized that the presence of the GFP tag results in the formation of less compact Httex1 inclusions. While Actin-F was found to colocalize with tag-free Httex1 inclusions [(Figure 1B, Httex1 72Q), 39Q (Figure S9D, Httex1 39Q), and ΔNt17 Httex1 72Q (Figure S10A, ΔNt17 Httex1 72Q)], no specific enrichment of Actin-F was detected in the core or periphery of the Httex1 72Q-GFP inclusions. Furthermore, actin filaments were found exclusively at the periphery of the tag-free Httex1 72Q and 39Q (+/- ΔNt17) cytoplasmic inclusions (Figures 1B and S10A). These results suggest a potential role of actin in the formation of Httex1 inclusion formation or maturation. Consistent with these observations, the actin cytoskeleton was one of the most dysregulated pathways according to a proteomic analysis conducted in human HD brains[98], underscoring its importance in the development of HD pathology.

Next, we performed a more in-depth analysis of the Httex1 72Q-GFP cellular inclusions formed in HEK by CLEM (Figure 7C-D). The Httex1 72Q-GFP inclusions were organized as a highly dense network of fibrils, which were more homogenously stained (Figures 7D and S16C) and did not exhibit the core and shell architecture that is characteristic of the tag-free Httex1 72Q inclusion (Figure 1D and S16D). Closer examination of the inclusions showed that they were composed of densely packed fibrils that exhibited a striking resemblance to the fibrillar aggregates formed by mutant Httex1 proteins in a cell-free system (Figures 7D and S16B). Structural analysis of Httex1 72Q-GFP by high-pressure freezing fixation (Figure S4B) also revealed densely packed fibrils radiating from the inclusions. The center of the inclusions was not well resolved, but thicker fibrils could clearly be observed radiating at the periphery with increased spacing between them compared to tag-free Httex1 72 inclusion (Figure S4A). A portion of Httex1 72Q-GFP inclusions exhibited perinuclear localization. In some cases, the accumulation of fibrils near the nuclear membrane leads to apparent

distortion of the nucleus but without membrane disruption (Figure 7D and S17A). Overall, we observed no significant differences in diameter and distance from the nucleus for all the Httex1 (+/-GFP) inclusions imaged in HEK cells (Figure S18).

Next, we investigated the ultrastructure properties of Httex1 72Q-GFP inclusions present in the nucleus of the HEK cells (Figures 7E-F). No significant differences in terms of organization were observed between nuclear and cytoplasmic Httex1 72Q-GFP inclusions by both GFP detection and antibody staining (Figure 7E). The Httex1 72Q-GFP nuclear inclusions were also enriched in fibrillar structures. The 3D reconstruction generated from the series of electron micrographs revealed much fewer membranous structures in both Httex1 39Q-GFP and Httex1 72Q-GFP inclusions (Figure S19) compared to tag-free Httex1 inclusions (Figures 1F and 1H). Moreover, consistent with EM observations, no neutral lipids were found in Httex1 39Q-GFP and Httex1 72Q-GFP inclusions (Figure S10B-C). Interestingly, neither the length of the polyQ repeat nor the presence or removal of the Nt17 domain seem to significantly alter the size, morphology or structural properties of the inclusions formed by mutant Httex1 proteins fused to GFP (Figure S20). This is different from what we observed for cells expressing tag-free Httex1, in which the increase of the polyQ length led to inclusions with distinct morphologies and organizational features. These findings suggest that the addition of GFP significantly alters the mechanism of Httex1 aggregation and inclusion formation.

To obtain an even clearer picture of these differences, we next performed EM under detergent-free conditions to preserve the internal membranes and structures of the inclusions. We observed that the length of the polyQ repeat did not influence the size of the Httex1 39Q-GFP and 72Q-GFP inclusions (Figure S18B) or their overall architecture in HEK cells. The Httex1 39Q-GFP inclusions are composed of radiating fibrils and are thus similar to the Httex1 72Q-GFP inclusions, although slightly less dense. The 3D reconstruction of the inclusions showed the presence of ER and mitochondria in their periphery, but few membranous structures were internalized (Figure S19B yellow arrowhead) as compared to

tag-free Httex1 39Q and Httex1 72Q inclusions. A similar analysis of Httex1 ΔNt17 39Q-GFP and Httex1 ΔNt17 72Q-GFP inclusions (found in cells) (FigureS20A-D) also revealed no effect of Nt17 deletion on the ultrastructure of the inclusions or their interactions with the surrounding organelles. These results confirm that mutant Httex1 aggregation and inclusion formation mechanisms are significantly altered by the addition of the GFP.

We also assessed how the presence of the GFP tag might influence the kinetics of aggregation, the morphology, subcellular localization and toxicity of the nuclear inclusions in primary cortical neurons (Figures 8 and S21). First, we observed that the presence of the GFP tag slows down the aggregation rate of Httex1 72Q: in contrast to the tag-free Httex1 72Q, the aggregation was significantly delayed, as evidenced by the absence of nuclear or cytoplasmic aggregates or inclusions at D3 (Figure 8A-B). However, at D7, almost all the Httex1 72Q-GFP proteins appeared in the form of small nuclear puncta (~35%) or large nuclear inclusions (~60%) (Figure 8C). The proportion of small puncta *vs.* large inclusions did not change over time, up to D14 (Figure 8C). Interestingly, the subcellular localization, the morphology and size distribution of the inclusions observed by confocal imaging were not impacted by the presence of the GFP tag. However, the Httex1 72Q-GFP aggregates exhibited a significantly reduced toxicity compared to tag-free Httex1 72Q in neurons (Figure S21D). Even at D14, chromatin condensation did not exceed 10% in these neurons (Figure S21D), whereas ~50% of the neurons overexpressing the tag-free Httex1 72Q construct were already dead (Figure 5E). In addition, the TUNEL cell death assay revealed a dramatic increase (~60%) in DNA fragmentation in the cortical neurons bearing the intranuclear Httex1 72Q inclusions compared to only 40% in neurons expressing Httex1 72Q-GFP (Figure 8D).

Next, we investigated how the presence of the GFP tag might impact the ultrastructural properties of these neuronal inclusions (Figures 8E and S22). The nuclear inclusions formed in the presence of the GFP tag exhibited a round shape but displayed a less dark staining density compared to the inclusions formed by the untagged Httex1 72Q protein (Figure 6A). Due to their lower density, the presence of filamentous structures organized as an entangled

arrangement throughout the GFP tagged inclusion could be detected. Finally, these inclusions were localized throughout the nucleus but always distant from the nuclear membrane (Figure S22).

Altogether, our results demonstrate that the addition of the GFP significantly slows the initiation of mutant Httex1 fibrillization and inclusion formation in the nucleus but accelerates the maturation of the aggregates once formed, resulting in predominantly large inclusions with reduced toxicity in neurons. The lack of physical interaction between the Httex1 72Q-GFP inclusions and the nuclear envelope and/or the absence of small puncta aggregates in neurons expressing Httex1-72Q-GFP could explain their reduced toxicity (Figures 8D-E).

The Httex1 72Q and Httex1 72Q-GFP nuclear and cytoplasmic inclusions exhibit distinct proteome composition

To gain further insight into the biochemical composition of the Htt nuclear inclusions, the molecular interactions and mechanisms driving their formation and maturation, we next investigated the proteome content of nuclear inclusions formed in primary neurons (Figure S23). Proteomic analysis showed that 23 proteins were significantly enriched in the Httex1 72Q inclusions compared to Httex1 16Q (Figure 8F). These proteins were analyzed by protein-protein association using the online platform STRING (Figure 8G) and classified using GO term analysis by Cellular component, Molecular function and Biological process (Figure S24). The proteins identified include the transcription factors PCBD2 and Mlf2, the RNA/DNA binding protein (GNL3), DNA-dependent RNA polymerase (Polr2c), histone lysine demethylase (No66), DNA genome nucleotide excision repair (Rad23B) and proteins linked to chromosome segregation (ARL8B and Tubb2a). In line with our results, ARL8B, Tubb2A, Polr2 sub-units, Mlf2, GNL3 and Rad23B proteins were also found enriched in the insoluble fractions of Q175 HD mice brains[99] and Tubb2a in R6/2 mice[100] nuclear inclusions. Interestingly, the gene expression level of these nuclear proteins was also significantly increased in HD post-mortem brain (PCBD2)[101] and symptomatic HD patients (Mlf2, GNL3,

Polr2 and ARL8B)[102]. Altogether, this suggests that the loss of key nuclear proteins due to their sequestration by the pathological Htt inclusion is compensated in neurons by increasing gene expression levels. However, this seems insufficient to compensate for the loss of their biological functions, as reflected by the high level of nuclear alterations observed in our neuronal HD model, including chromatin condensation, nuclear fragmentation, and nuclear envelope integrity loss (Figure 6).

In addition to the nuclear proteins, STRING analysis (Figure 8G), together with GO term classification of cellular components (Figure S24A), the molecular functions (Figure S24B), and the biological process annotations (Figure S24C) revealed the enrichment of a cluster of proteins [Ubiquilin (ubqln) 1, 2 and 4; Rps27a, Rad23B and Nedd8, red circle, Figure 8G] related to the protein degradation machinery, including the UPS, autophagy and ERAD pathways. In line with our findings, all these proteins were also found enriched in the insoluble fractions of the Q175 HD mice brains, while the Ubiquilin family members (Ubqln 1, 2 or 4)[103–105] were also shown to be sequestered in R6/2 mice nuclear inclusions[100] and in the Httex1 nuclear inclusions formed in the PC12 neuronal rat precursor[106]. Interestingly, ubiquilin proteins have been previously shown to translocate from the cytoplasm to the nucleus or have an upregulated expression level in the nucleoplasm concomitantly with the early stage of the formation of the neurofibrillary tangles in AD post-mortem brain tissues[107]. Furthermore, Nedd8, originally shown to colocalize with ubiquitin and the proteasome components in the cytoplasmic inclusions[108,109] found in several neurodegenerative disorders, has recently been shown to promote nuclear protein aggregation as a defense mechanism against proteotoxicity[110]. Moreover, our analysis revealed 5 proteins known as Htt interactors (based on the HDinHD dabase) among the proteins significantly different between Httex1 72Q compared to Httex1 16Q in primary neurons (Table S1).

Finally, we also assessed how the presence of the GFP tag might influence the protein content of the neuronal intranuclear inclusions (Figure 8H). Similar to the Httex1 72Q aggregates, ~45% of the proteins enriched in the insoluble fraction of the Httex1 72Q-GFP

aggregates were related to nuclear biological processes and functions, including transcription factors (Mlf2[106], nfyc-1, TCERG1, Med15), DNA-chromatin binding proteins (ZBED5, N6AMT1 and Actl6b), DNA genome nucleotide excision repair protein (Rad23B), the DNA/RNA-binding protein FUS. In addition, Httex1 72Q-GFP aggregates were also enriched in proteins from the promyelocytic leukemia nuclear bodies (Sumo 1 and 2) known as nuclear membraneless compartments involved in genome maintenance such as DNA repair, DNA damage response, telomere homeostasis, and which is also associated with apoptosis signaling pathways (Figure S25). Furthermore, proteins from the ubiquitin-proteasome system (Bag5, Fus, Rad23b, Sgta, Sumo1, Sumo2, Ubqln1, Ubqln2, Ubqln4), the ERAD (Sgta, Ubqln1, Ubqln2), autophagy (Ubqln1, Ubqln2, Ubqln4) and sumoylation (Sumo1, Sumo2) pathways were also highly enriched in the insoluble fraction of the Httex1 72Q-GFP aggregates (Figure S25A-B). Interestingly, the proteome of the Httex1 72Q-GFP aggregates formed in our HD neuronal model shared 40% of the proteins also found enriched in the insoluble fraction of Httex1 74Q-GFP nuclear inclusions formed in the PC12 neuronal rat precursor cell line[106]. This highlights a strong similarity between the pathways and proteins involved in the aggregation of Httex1 and inclusion formation in rodent neuronal cells.

We next compared the proteins identified between tag-free Httex1 72Q inclusions and Httex1 72Q-GFP (Figure 8I). 24 proteins were unique to Httex1 72Q (44.4%), 17 unique to Httex1 72Q-GFP (31.5%) and only 13 (24.1%) common to both type of inclusions. Most of the unique proteins found in the tag-free or GFP-tagged Httex1 72Q inclusions were related to nuclear functions, the ubiquitin-proteasome system, ERAD and autophagy pathways. Moreover, among the 13 common proteins, most were linked to the protein degradation machinery (i.e., ubiquilins 1, 2 and 4, and the Rad23b and Nedd8 proteins).

Although the tag-free Httex1 72Q and Httex1 72Q-GFP inclusions share several proteins related to the degradation machinery, more than 75% of the co-aggregating proteins are different, which could explain the drastic differences in neuronal toxicity associated with each type of these inclusions.

As the majority of the inclusions formed in neurons are nuclear, we used HEK cells to further assess how the GFP tag influences the proteome of the cytoplasmic Httex1 inclusions (Figure S11A). Volcano plot analysis showed 492 proteins significantly enriched in the insoluble fraction of the HEK cells overexpressing Httex1 72Q-GFP as compared to those expressing GFP (Figure 9A). We observed a significant enrichment of the endogenous HTT protein, suggesting that, as for the tag-free Httex1 72Q, mutant Httex1-GFP inclusions can recruit the endogenous HTT protein (Figure S11E).

The cytoplasmic components enriched in the insoluble fraction of Httex1 72Q-GFP were similar to those found with tag-free Httex1-72Q and were part of the endomembrane system (~50%, light blue Figure 9B), the cytoskeleton, the perinuclear region, the UPS, mRNA processing bodies, and stress granules (Figure 9B, dark blue). However, in contrast to the tag-free Httex1 72Q insoluble fractions, in which no mitochondrial protein was found to be enriched, 10% of the proteins enriched in the Httex1 72Q-GFP insoluble fraction were related to the mitochondria compartment (purple Figure 9B). The nuclear proteins found in the Httex1 72Q-GFP insoluble fraction belong to similar nuclear compartments as those identified previously in the Httex1 72Q insoluble fraction (Figure 9B, grey).

Biological process (Figure S26) and canonical pathway (Figure S27) analyses revealed that the UPS and chaperone machinery were the most enriched terms, as previously observed in the tag-free insoluble fraction. This indicates that the process of aggregation of Httex1 itself, regardless of the presence of the GFP tag, leads to the sequestration of the key cellular machinery responsible for protein folding and protein degradation. This could compromise the cell's ability to prevent the accumulation or clearance of Httex1 aggregates. Although in different proportions, most of the biological processes and pathways significantly enriched in the tag-free Httex1 72Q insoluble fraction, such as inflammation, transcription, HD signaling, and cell death, were also detected in the Httex1 72Q-GFP insoluble fraction.

Having identified the proteins significantly enriched in both tag-free and GFP-tag 72Q inclusions, we next determined which proteins were unique to each type of inclusion. Toward

this goal, we used a Venn diagram to compare the lists of proteins significantly enriched in our volcano plot analyses [(Httex1 72Q vs. Httex1 16Q insoluble fractions) vs. (Httex1 72Q-GFP vs. Httex1 16Q insoluble fractions)] (Figures 3A and S11C). Figure 9C shows that ~45% (256 proteins) were found in both the tag-free and the GFP-tag Httex1 72Q inclusions. In total, 120 proteins (20.9%) were unique to the Httex1 72Q insoluble fraction, and 198 proteins (34.5%) were unique to the Httex1 72Q-GFP. Overall, we found 55% different proteins among the proteins that co-aggregate with or are sequestered in Httex1 72Q vs. 72Q-GFP inclusions, both compared to Httex1 16Q. We used the Kyoto Encyclopedia of Genes and Genomes (KEGG) pathway analysis to classify the list of proteins in Httex1 inclusions (Figure 9D). The proteasome, protein processing in the endoplasmic reticulum, and endocytosis were among the most enriched pathways from the common co-aggregated proteins. Those 3 terms were also enriched significantly for Httex1 72Q-GFP, indicating the involvement of other unique proteins enriched in those pathways compared to Httex1 72Q. The KEGG classification revealed two distinct clusters for Httex1 72Q and Httex1 72Q-GFP, as well as additional differences (Figure 9D). Proteins related to infection and inflammatory pathways (e.g., Herpes simplex infection, TNF signaling, and Toll-like receptor signaling) were found to be unique to Httex1 72Q, whereas proteins related to metabolism were specifically enriched for Httex1 72Q-GFP. Our proteomic analysis highlights that the addition of a fluorescent tag such as GFP significantly alters not only the mechanism of Htt inclusion formation but also the Htt interactome and thus the biochemical composition of inclusions.

Httex1 72Q inclusions induce higher respirational dysfunction and a stronger decrease of ERES number compared to Httex1 72Q-GFP in HEK cells

Next, we investigated how the aggregation of mutant Httex1-GFP and the formation of cytoplasmic inclusions affect the mitochondrial and ER-related functions. First, we measured the mitochondrial respiration in different respirational states in HEK cells (Figure S13C-D). Compared to our findings with the tag-free mutant Httex1-72Q (Figure 4C), the increased

mitochondrial respiration was significant but less pronounced for Httex1 72Q-GFP than for Httex1 16Q-GFP (Figure S13E). Given the role of mitochondria as a major source of reactive oxygen species (ROS), with implications of ROS in both neurodegenerative disease and cellular protective signaling cascades[111,112], we suspected that mitochondrial ROS production might be affected by the mitochondrial fragmentation observed in regions close to tag-free Httex1 72Q and absent for Httex1 72Q-GFP (Figure S28A-B). To test this hypothesis, we used an amplex red assay to measure mitochondrial ROS (superoxide and hydrogen peroxide) production concurrent with mitochondrial respiration (Figure S13D). We observed no significant differences in mitochondrial ROS production between the tag-free or GFP tagged Httex1 72Q or 16Q (Figure S28C).

Mitochondrial fragmentation[113] and inflammation[114] are hallmarks of Htt-induced neurodegeneration. Recent studies reported the major role of mitochondrial fission and fusion homeostasis in HD and also revealed the specific mitochondrial fragmentation induced by mutant Htt using electron microscopy in STHdh neurons[115,116]. Interestingly, only tag-free Httex1 72Q overexpression results in mitochondrial fragmentation and is characterized by the strong accumulation of inflammation-linked proteins in the aggregates. We speculate that the observed hyper-activation of mitochondrial respiration (in the absence of significantly increased ROS production) is an adaptation of the inclusion-bearing cells in order to generate sufficient energy by oxidative phosphorylation for increased energetic demands for unfolding or clearance of aggregating proteins. A similar hyperactivation of mitochondrial respiration has recently been reported for alpha-synuclein aggregates[117]. These authors hypothesized that the hyper-respiration might represent a pathogenic upstream event to alpha-synuclein pathology. We think that this may also be the case for untagged Httex1 72Q induced pathology. However, based on our extensive proteomic analyses of the inclusions formed by Httex1 72Q to or Httex1 72Q-GFP and the possibility of comparing the functionality of organelles in our cellular model, we can provide a more elaborate hypothesis. In the tag-free Httex1 72Q condition, mitochondrial hyperactivity coincided with both

mitochondrial fragmentation and the detection of more inflammation-related proteins in the aggregates as compared to the GFP condition. We speculate that mitochondrial fragmentation initially may be protective, as it enhances mitochondrial mobility necessary for cell repair processes[118]. Upregulation of mitochondrial respiration would be a reasonable consequence of elevated ATP-requirements for mitochondrial and protein transport related to aggregation formation and proteostatic processes including ATP-requiring chaperone-, proteasome and autophagy processes.

Finally, we also investigated whether Httex1-GFP inclusions interfere with the homeostasis of ERES by comparing the size and the number of ERES in HeLa cells overexpressing Httex1 16Q-GFP to those expressing mutants GFP-tagged Httex1 39Q or 72Q (Figure S29A). We found that cells containing Httex1 72Q-GFP inclusions caused a decrease in ERES number (Figure S29B, upper panel), although non-significant, compared to Httex1 72Q, which showed a 20% reduction (Figure 4E, upper panel). The reduction of ERES size was significant for cells expressing Httex1 72Q-GFP but not Httex1 39Q-GFP compared to Httex1 16Q-GFP (Figure S29B, lower panel). Thus, the effect of Httex1-GFP inclusions on ERES is present but is less pronounced compared to that observed in cells containing tag-free Httex1 inclusions. These observations are consistent with recent cryo-ET studies suggesting decreased ER dynamics near Httex1-GFP inclusions[12].

Overall, our results show that the cellular organelle responses and adaptation to inclusion formation were different for the Httex1 72Q-GFP inclusions than for the Httex1 72Q inclusions, consistent with the GFP-dependent changes observed in the proteome and the ultrastructural properties of Httex1 cytoplasmic inclusions.

Discussion

Cytoplasmic Httex1 inclusion formation and maturation involves a complex interplay between Httex1 aggregates and organelles

Pathological inclusions in neurodegenerative diseases have been shown to have a complex organization and composition. For example, it has been recently demonstrated that Lewy bodies (LB) isolated from Parkinson's disease brains or LB-like inclusions in primary neurons are composed of not only filamentous and aggregated forms of alpha-synuclein but also a complex milieu of lipids, cytoskeletal proteins, and other proteins and membranous organelles, including mitochondria and autophagosomes[119–122]. Studies in neuronal cultures also showed that the recruitment of lipids and membranous organelles during LB formation and maturation contribute to organelles' dysfunctions and lead to synaptic dysfunction and neurodegeneration. In line with these findings, our EM data, together with 3D reconstruction, revealed the presence of membrane fragments and vesicles entrapped in the core of the Httex1 inclusions. Consistent with these observations, our proteomic analysis revealed that 24% of the proteins enriched in the inclusions fraction belong to the endolysosomal compartments, the Golgi apparatus and the trans-Golgi network (Figure 3). In addition, mitochondria and ER were found in the periphery of inclusions, as previously reported in cellular models[15] and human tissue[95,123]. We hypothesized that sequestration of key functional proteins, together with lipids, endomembranes and organelles inside the Httex1 inclusions, could challenge cellular homeostasis. In line with this hypothesis, our electron micrographs revealed that the mitochondria associated with Httex1 72Q inclusions were fragmented and often exhibited disorganized or depleted cristae (Figure 4A). These changes in mitochondrial morphology were associated with dysregulation of the mitochondrial respiration (Figure 4C), consistent with previous studies demonstrating that mutant Htt aggregates interact directly with outer mitochondrial membranes (in STHdh cells)[124] and induce mitochondrial fragmentation (in primary neurons)[125]. Defects in mitochondrial

respiration have also been observed in HD patients' brains, especially defects of complexes II and IV of the respiratory chain may impair oxidative phosphorylation[126–128].

The ER at the periphery of the Httex1 72Q inclusions were also affected at the structural level, as shown by their morphological reorganization in rosette or “stacked cisternae”, and at the functional level, as evidenced by the dysregulation of the ERES homeostasis (Figure 4D-E). The formation of ER rosettes indicates the accumulation of proteins in the smooth ER[92] and is thought to result from low-affinity binding and export defects, which can be caused by unfolded Htt proteins but is not necessarily linked to ER stress. Kegel and colleagues[129] also reported the presence of ER cisternae next to aggregates formed by the expression of a large Htt fragment fused to a FLAG tag in clonal striatal cells. The formation of Httex1 inclusions seems to drive the reorganization of the ER network in their periphery but did not lead to ER protein sequestration, as shown by the quantitative proteomic analysis, which did not reveal significant ER proteins trapped inside the inclusions. The presence of ribosomes and ER membrane deformation was previously detected close to the periphery of Httex1 inclusions by cryo-ET[12] and was linked to a strong reduction in ER dynamics. In the same study[12], the periphery of the inclusions was immunoreactive to several components of the ER-associated degradation (ERAD) machinery (e.g., Erlin-2, Sel1L). These observations are consistent with our ICC data showing the presence of ER chaperone BIP at the outer periphery but not inside the inclusions (Figure S5). We also observed ERES modulation, which can be explained by the sequestration of specific proteins required for their fusion[130]. Consistent with these observations, our proteomic analysis showed the enrichment of proteins specific to the ER-Golgi trafficking. ERES modulation can also be explained by a reduction of the biosynthetic capacity of this compartment, as ERES have been shown to adapt to the amount of secretory burden to which they are exposed[131]. The recruitment and perturbation of the ER network might contribute to cytotoxicity during inclusion formation, but on its own does not appear to be sufficient to cause overt toxicity. Consistent with this

hypothesis, the ERAD and Ca^{2+} signaling pathways have been extensively reported to be dysregulated in various cellular and animal models using different Htt fragments[132–137].

Cytoplasmic and nuclear Htt inclusions exhibit distinct ultrastructural properties that are differentially influenced by the size of the polyQ repeats

Although previous studies have suggested the formation of ring-like nuclear inclusions, this architecture was defined by the peripheral staining of nuclear proteins and not by the peripheral staining of Htt as observed in the case of cytoplasmic inclusions (Figure 1). Our in-depth characterization of the Httex1 72Q inclusions at the ultrastructure level revealed distinct differences in the organization and architecture between the cytoplasmic and nuclear Htt inclusions. The cytoplasmic Httex1 72Q inclusions exhibit a dense core and shell morphology and are composed of highly organized fibrillar aggregates in both the core and the periphery. In contrast, nuclear Htt inclusions, in both HEK cells or primary cortical neurons, exhibited less complex ultrastructural properties, appeared as homogenous structures without the core and periphery morphology and were devoid of endomembranes or vesicles (Figures 2 and 6A). These observations are consistent with most of the Htt nuclear inclusions found in HD mice models, which do not display the core and shell organization[19,32].

Our new data on nuclear neuronal Htt inclusion revealed that tag-free mutant Httex1 expression in primary neurons leads to the formation of granulo-filamentous nuclear inclusions, similar to previous ultrastructural studies performed in HD patients brains and *in vivo* models of HD, including R6/2 mice[19,32] and transgenic rat[138]. However, in most of these studies, the ultrastructural properties of the filaments were less evident compared to the well-resolved filamentous structure we and others[12] showed using electron tomography. For example, Tagawa and colleagues also observed nuclear inclusions of tag-free Httex1, but their data did not reveal the level of ultrastructural details and insights that our study provides[139].

Our results also suggest that the intracellular environment and interactions with lipids and endomembranes or vesicles are key determinants of the structural and molecular complexity of the inclusions and that different mechanisms drive the formation and maturation of the nuclear and cytoplasmic inclusions. Such differential characteristics between cytoplasmic and nuclear inclusions might account for the differential cellular dysfunction and toxicity associated with these two types of Htt inclusions[29,140–143]. Furthermore, the differential toxicity seen for Htt nuclear inclusions in primary neurons compared to HEK 293 cells indicate a cell-type dependent Htt toxicity that might arise from distinct Htt mechanisms of aggregation or interaction with cellular proteins or differences in the resilience of the different cells based for example on distinct oxidative stress tolerance and immune functions/inflammation.

We speculate that the formation of the core of the inclusions is guided predominantly by intermolecular interactions involving the polyQ domain and could be initiated by rapid events that are potentially driven by phase separation, as recently described by several groups[14,39,144,145]. The rapid formation of the aggregate's core does not allow for the regulated recruitment of other proteins and organelles (Figures 1, 2 and 10A), as evidenced by the fact that most antibodies against proteins found in Htt inclusion stain the periphery rather than the core of the inclusions[48]. The Nt17 domain most likely plays key roles in the initial oligomerization events and, possibly, the packing or lateral association of the fibrils. Once this core of dense fibrils is formed, the fibrils at the periphery continue to grow through the recruitment of endogenous soluble proteins (Figures 3 and 10A). Because this growth phase is slower, it allows the fibrils to interact with and/or recruit other proteins into the inclusions. Consistent with this hypothesis, Matsumoto and colleagues showed that the transcription factors TATA-binding protein (TBP) and CREB-binding protein (CBP)—containing a polyQ expansion—were present only at the periphery of the inclusions and not in the core[47]. Interestingly, although the length of the polyQ repeat did not seem to significantly influence the density of the fibrils at the core of the inclusions, the peripheral organization of the Htt

fibrils and the formation of the outer shell showed strong polyQ repeat length dependence (Figures 4 and 10A). This model is supported by studies from Hazeki *et al.* and Kim *et al.,* demonstrating that the detergent-insoluble core of cellular Httex1 inclusions represents the skeletal structure of the inclusions, while the active surface dynamically interacts with Htt species and proteins being processed[30,38]. Altogether, our results highlight that the formation of Htt inclusions occurs in two major phases with, first, the formation of the core driven primarily by the polyQ repeat domain, and then the growth of the inclusions with the addition of Htt fibrils and the recruitment of other proteins and organelles. The second phase appears to be driven by interactions involving both the polyQ and PRD domains and involves the active recruitment and sequestration of lipids, proteins, and membranous organelles (Figure 10A)**.** However, we cannot rule out the presence of entrapped oligomers in the core or at the surface close to the growing fibrils in the periphery[146]. Previously, Qin *et al*., using a FLAG-tagged Htt1-969 fragment (100Q), demonstrated that the Htt species in the core of the inclusions are highly protease-resistant and that oligomeric forms of Htt accumulate with cytoplasmic proteins and vesicles in the periphery of the inclusions[48].

The fusion of fluorescent proteins to mutant Httex1 significantly alters the biochemical and structural properties of mutant Htt

To the best of our knowledge, this is the first study to directly compare inclusions formed by tag-free mutant native Httex1 proteins to GFP-tagged mutant Httex1 at the structural, interactome and biochemical levels.

The ultrastructure of Httex1 72Q-GFP inclusions revealed radiating fibrils with homogenous staining and the absence of the core and shell morphology. In line with our findings, previous studies showed that cytoplasmic Httex1 72Q-GFP aggregates are fibrillar[14,147] and resemble other Httex1-GFP aggregates in COS cells[148], in primary striatal neurons[149] as well as aggregates formed by mutant Httex1 fused to a FLAG tag in HEK cells[15]. In a recent cryo-electron tomography (Cryo-ET) study, Bäuerlein *et al.* examined the ultrastructural properties

of mutant Httex1 in the absence and presence of GFP and suggested that the presence of GFP does not significantly alter the organization of the cytoplasmic inclusions in HeLa and neurons[12]. Similar to our findings, they showed that the presence of the GFP tag 1) induces a 50% reduction in fibril density and a 25% increase in fibril stiffness; 2) results in increased spacing between the fibrils in the Httex1-GFP inclusions; and; 3) does not influence the overall size of the inclusions. However, when it comes to the ultrastructural properties of the tag-free mutant Httex1 inclusions, we observed very different results, as they did not observe the formation of inclusions with core and shell morphologies. Examination of the sequence of the constructs they used reveals a Myc-tag at the N-terminal side of their Httex1 proteins, whereas the constructs we used contain only the native sequence of mutant Httex1. While we showed that removal of the Nt17 domain does not influence the ability of tag-free Htt to form inclusions with the core and shell organization, the fusion of additional amino acids in the N-terminus could still significantly alter the kinetics, oligomerization, and aggregation pathway of Httex1 protein. In addition to differences at the ultrastructural levels, our studies showed the recruitment of membranous organelles and vesicles as disrupted structures inside the inclusions in both the core and shell but also in the form of intact ER-mitochondrial network at the periphery of the tag-free inclusions. Less internalized structures were observed in the Httex1-GFP inclusions, consistent with the findings of Bäuerlein *et al.*[12]. Another major difference between the two studies is that Bäuerlein *et al.* did not observe any polyQ-length effect on the size or ultrastructural properties of the inclusions formed by mutant Httex1-GFP over the polyQ repeat range of 64Q to 97Q. Although the presence of GFP can explain the differences between the two results, it is also possible that these differences are because the authors compared polyQ repeats that are far beyond the pathogenic threshold. We think that in this polyQ range, the difference in aggregation properties between 64 and 97Q would be small compared to what one would observe when comparing mutant Httex1 with polyQ repeats close to the pathogenic threshold (39-43Q). Therefore, in our study, we compared the ultrastructure properties of the inclusions of Httex1 containing 39 or 72Q repeats. In our experiments, the cytoplasmic inclusions formed by

mutant Httex1 39Q were found to be less organized and did not exhibit a stable core and shell arrangement as in the case of Httex1 72Q. Finally, in primary neurons, the use of Httex1 72Q-GFP changed dramatically the kinetics of inclusion formation and the proportion of small and large nuclear aggregates compared to tag-free Httex1 72Q. Moreover, neuronal Httex1 72Q-GFP nuclear inclusions were smaller and less dense compared to the tag-free Httex1 72Q inclusions, exhibited a distinct proteome composition and interracted less with the nuclear membrane. These differences could explain the reduced toxicity of Httex1 72Q-GFP inclusions compared to tag-free Httex1 72Q inclusions.

Altogether, our data suggest that the aggregation processes of tag-free and GFP-tagged Httex1 are distinct (Figures 10B and S30), thus underscoring the potential limitations of using GFP to investigate the molecular, biochemical, and cellular determinants of Htt inclusion formation and mechanisms of toxicity.

Conclusion

In summary, our integrative imaging and proteomic studies demonstrate that the process of Htt cytoplasmic inclusion formation occurs in at least two phases and involves the active recruitment of lipids, proteins, and organelles. The organization and ultrastructural properties of these inclusions are greatly influenced by the polyQ repeat length and the intracellular environment, as evidenced by the fact that cytoplasmic and nuclear Httex1 inclusions exhibit distinct ultrastructural properties. Equally important, our work emphasizes the importance of elucidating the role of Htt interactions with lipids and membranous organelles in regulating the process of Htt aggregation, inclusion formation, and toxicity. Extending the studies and approaches presented here to other HD model systems and other Htt fragments, will pave the way to a better understanding of the mechanisms of Htt inclusion formation and how it contributes to the development of HD. We recently demonstrated that Htt171 aggregates *in vitro* via different mechanisms that are distinct from Httex1 and that the structured domains outside exon1 could play important roles in regulating early events associated with Htt

oligomerization, initiation of Htt aggregation and inclusion formation[150]. This will also enable a more effective use of appropriate models to assess the therapeutic potential of targeting different stages and mechanisms of Htt inclusion formation and maturation.

Taken together, our work provides important and novel insights that not only advance our understanding of the mechanisms of Htt aggregation but also point to new directions for therapeutic interventions. We show that Htt aggregation and inclusion formation in the cytosol and nucleus occur via different mechanisms and lead to the formation of inclusions with distinct biochemical and ultrastructural properties. These observations suggest that the two types of inclusions may exert their toxicity via different mechanisms and may require different strategies to interfere with their formation, maturation and toxicity. Furthermore, our work suggests that identifying modifiers of Htt inclusion growth and aberrant secondary interactions with other proteins and organelles represent an alternative and strategy for interfering with Htt-induced toxicity and slowing disease progression, especially after disease onset. Therefore, we believe that targeting inclusion growth and maturation represents a viable therapeutic strategy.

References

1. Cattaneo E, Rigamonti D, Goffredo D, Zuccato C, Sipione S, Cattaneo E. Loss of normal huntingtin function□: new developments in Huntington ' s disease research. *TRENDS Neurosci*. 2001;24(3):182-188.
2. Ross C a, Aylward EH, Wild EJ, et al. Huntington disease: natural history, biomarkers and prospects for therapeutics. *Nat Rev Neurol*. 2014;10(4):204-216. doi:10.1038/nrneurol.2014.24
3. Stout JC, Paulsen JS, Queller S, et al. Neurocognitive Signs in Prodromal Huntington Disease. *Neuropsychology*. 2012;25(1):1-14. doi:10.1037/a0020937.Neurocognitive
4. Macdonald ME, Ambrose CM, Duyao MP, et al. A Novel Gene Containing a Trinucleotide That Is Expanded and Unstable on Huntington ' s Disease Chromosomes. *Cell*. 1993;72:971-983.
5. Kremer B, Goldberg P, Andrew SE, et al. A worldwide study of the huntington's disease mutation. *N Engl J Med*. 1994;330(20):1401-106.
6. Lee J, Ramos EM, Lee J, Gillis T. CAG repeat expansion in Huntington disease determines age at onset in a fully dominant fashion. *Neurology*. 2012;78(10):690-695.
7. Lee JM, Correia K, Loupe J, et al. CAG Repeat Not Polyglutamine Length Determines Timing of Huntington's Disease Onset. *Cell*. 2019;178(4):887-900.e14. doi:10.1016/j.cell.2019.06.036
8. James R. Arndta, Maxmore Chaibvaa, and Justin Legleitera, b, c At. The emerging role of the first 17 amino acids of huntingtin in Huntington's disease. *Biomol Concepts*. 2016;8(5):583-592. doi:10.1002/aur.1474.Replication
9. Atwal RS, Xia J, Pinchev D, Taylor J, Epand RM, Truant R. Huntingtin has a membrane association signal that can modulate huntingtin aggregation, nuclear entry and toxicity. *Hum Mol Genet*. 2007;16(21):2600-2615. doi:10.1093/hmg/ddm217
10. Thompson LM, Aiken CT, Kaltenbach LS, et al. IKK phosphorylates Huntingtin and targets it for degradation by the proteasome and lysosome. *J Cell Biol*. 2009;187(7):1083-1099. doi:10.1083/jcb.200909067
11. Shen K, Calamini B, Fauerbach JA, et al. Control of the structural landscape and neuronal proteotoxicity of mutant Huntingtin by domains flanking the polyQ tract. *Elife*. 2016;5:e18065. doi:10.7554/eLife.18065
12. Bäuerlein FJB, Saha I, Mishra A, et al. In Situ Architecture and Cellular Interactions of PolyQ Inclusions. *Cell*. 2017;171(1):179-187.e10. doi:10.1016/j.cell.2017.08.009
13. Gruber A, Hornburg D, Antonin M, et al. Molecular and structural architecture of polyQ aggregates in yeast. *Proc Natl Acad Sci*. 2018;115(15):E3446-E3453. doi:10.1073/pnas.1717978115
14. Peskett TR, Rau F, O'Driscoll J, Patani R, Lowe AR, Saibil HR. A Liquid to Solid Phase Transition Underlying Pathological Huntingtin Exon1 Aggregation. *Mol Cell*. 2018;70(4):588-601. doi:10.1016/j.molcel.2018.04.007
15. Waelter S, Boeddrich A, Lurz R, et al. Accumulation of mutant huntingtin fragments in aggresome-like inclusion bodies as a result of insufficient protein degradation. *Mol Biol Cell*. 2001;12(5):1393-1407. doi:10.1091/mbc.12.5.1393
16. Neueder A, Landles C, Ghosh R, et al. The pathogenic exon 1 HTT protein is produced by incomplete splicing in Huntington's disease patients. *Sci Rep*. 2017;7(1):1307. doi:10.1038/s41598-017-01510-z
17. Wellington CL, Ellerby LM, Gutekunst C-A, et al. Caspase cleavage of mutant huntingtin precedes neurodegeneration in Huntington's disease. *J Cell Biol*. 2002;22(4):749-759. doi:10.1038/35096019
18. Schilling G, Klevytska A, Tebbenkamp ATN, et al. Characterization of huntingtin pathologic fragments in human Huntington disease, transgenic mice, and cell models. *J Neuropathol Exp Neurol*. 2007;66(4):313-320. doi:10.1097/nen.0b013e318040b2c8
19. Davies SW, Turmaine M, Scherzinger E, Wanker EE, Mangiarini L, Bates GP. Formation of Neuronal Intranuclear Inclusions Underlies the Neurological Dysfunction in Mice Transgenic for the HD Mutation. *Cell*. 1997;90:537-548.

20. Mangiarini L, Sathasivam K, Seller M, et al. Exon I of the HD gene with an expanded CAG repeat is sufficient to cause a progressive neurological phenotype in transgenic mice. *Cell*. 1996;87(3):493-506. doi:10.1016/S0092-8674(00)81369-0
21. Martindale D, Hackam A, Wieczorek A, et al. Length of huntingtin and its polyglutamine tract influences localization and frequency of intracellular aggregates. *Nat Genet*. 1998;18(3):150-154. doi:10.1038/ng0598-51
22. Barbaro BA, Lukacsovich T, Agrawal N, et al. Comparative study of naturally occurring Huntingtin fragments in Drosophila points to exon 1 as the most pathogenic species in Huntington's disease. *Hum Mol Genet*. 2015;24(4):913-925. doi:10.1093/hmg/ddu504
23. Wang H, Lim PJ, Yin C, Rieckher M, Vogel BE, Monteiro MJ. Suppression of polyglutamine-induced toxicity in cell and animal models of Huntington's disease by ubiquilin. *Hum Mol Genet*. 2006;15(6):1025-1041. doi:10.1093/hmg/ddl017
24. Luo H, Cao L, Liang X, Du A, Peng T, Li H. Herp Promotes Degradation of Mutant Huntingtin: Involvement of the Proteasome and Molecular Chaperones. *Mol Neurobiol*. 2018;55(10):7652-7668. doi:10.1007/s12035-018-0900-8
25. Scherzinger E, Sittler A, Schweiger K, et al. Self-assembly of polyglutamine-containing huntingtin fragments into amyloid-like fibrils: implications for Huntington's disease pathology. *Proc Natl Acad Sci U S A*. 1999;96(8):4604-4609. doi:10.1073/pnas.96.8.4604
26. Rockabrand E, Slepko N, Pantalone A, et al. The first 17 amino acids of Huntingtin modulate its sub-cellular localization, aggregation and effects on calcium homeostasis. *Hum Mol Genet*. 2007;16(1):61-77. doi:10.1093/hmg/ddl440
27. Steffan JS, Agrawal N, Pallos J, et al. SUMO modification of Huntingtin and Huntington's disease pathology. *Science*. 2004;304(5667):100-104. doi:10.1126/science.1092194
28. Tam S, Spiess C, Auyeung W, et al. The chaperonin TRiC blocks a huntingtin sequence element that promotes the conformational switch to aggregation. *Nat Struct Mol Biol*. 2009;16(12):1279-1285. doi:10.1038/nsmb.1700
29. Zheng Z, Li A, Holmes BB, Marasa JC, Diamond MI. An N-terminal nuclear export signal regulates trafficking and aggregation of huntingtin (Htt) protein exon 1. *J Biol Chem*. 2013;288(9):6063-6071. doi:10.1074/jbc.M112.413575
30. Kim YE, Hosp F, Frottin F, et al. Soluble Oligomers of PolyQ-Expanded Huntingtin Target a Multiplicity of Key Cellular Factors. *Mol Cell*. 2016;63(6):950-964. doi:10.1016/j.molcel.2016.07.022
31. Lu M, Banetta L, Young LJ, et al. Live-cell super-resolution microscopy reveals a primary role for diffusion in polyglutamine-driven aggresome assembly. *J Biol Chem*. 2019;294(1):257-268. doi:10.1074/jbc.RA118.003500
32. Scherzinger E, Lurz R, Turmaine M, et al. Huntingtin encoded polyglutamine expansions form amyloid-like protein aggregates in vitro and in vivo. *Cell*. 1997;90(3):549-558. http://discovery.ucl.ac.uk/21647/.
33. Hollenbach B, Scherzinger E, Schweiger K, Lurz R, Lehrach H, Wanker EE. Aggregation of truncated GST--HD exon 1 fusion proteins containing normal range and expanded glutamine repeats. *Philos Trans R Soc B Biol Sci*. 1999;354(1386):991-994. doi:10.1098/rstb.1999.0450
34. Ansaloni A, Wang ZM, Jeong JS, Ruggeri FS, Dietler G, Lashuel HA. One-pot semisynthesis of exon 1 of the Huntingtin protein: New tools for elucidating the role of posttranslational modifications in the pathogenesis of Huntington's disease. *Angew Chemie - Int Ed*. 2014;53(7):1928-1933. doi:10.1002/anie.201307510
35. Thakur AK, Jayaraman M, Mishra R, et al. Polyglutamine disruption of the huntingtin exon1 N-terminus triggers a complex aggregation mechanism Ashwani. *Nat Struct Mol Biol*. 2009;16(4):380-389. doi:10.1038/nsmb.1570.Polyglutamine
36. Gu X, Greiner ER, Mishra R, et al. Serines 13 and 16 Are Critical Determinants of Full-length Human Mutant Huntingtin-Induced Disease Pathogenesis in HD Mice. *Neuron*. 2009;64(6):828-840. doi:10.1016/j.neuron.2009.11.020.Serines
37. Maiuri T, Woloshansky T, Xia J, Truant R. The huntingtin N17 domain is a

multifunctional CRM1 and ran-dependent nuclear and cilial export signal. *Hum Mol Genet*. 2013;22(7):1383-1394. doi:10.1093/hmg/dds554
38. Hazeki N, Tsukamoto T, Yazawa I, et al. Ultrastructure of nuclear aggregates formed by expressing an expanded polyglutamine. *Biochem Biophys Res Commun*. 2002;294(2):429-440. doi:10.1016/S0006-291X(02)00498-9
39. Aktar F, Burudpakdee C, Polanco M, et al. The huntingtin inclusion is a dynamic phase-separated compartment. *Life Sci Alliance*. 2019;2(5):1-14. doi:10.26508/lsa.201900489
40. Miao K, Wei L. Live-Cell Imaging and Quantification of PolyQ Aggregates by Stimulated Raman Scattering of Selective Deuterium Labeling. *ACS Cent Sci*. 2020. doi:10.1021/acscentsci.9b01196
41. Sophie Vieweg, Mahul-Mellier A-L, Ruggeri FS, et al. Towards deciphering the Nt17 code: How the sequence and conformation of the first 17 amino acids in Huntingtin regulate the aggregation, cellular properties and neurotoxicity of mutant Httex1. *bioRxiv*. 2021:6.
42. Iwata A, Riley BE, Johnston JA, Kopito RR. HDAC6 and microtubules are required for autophagic degradation of aggregated Huntingtin. *J Biol Chem*. 2005;280(48):40282-40292. doi:10.1074/jbc.M508786200
43. Mantha N, Das NG, Das SK. Recent Trends in Detection of Huntingtin and Preclinical Models of Huntington's Disease. *ISRN Mol Biol*. 2014;2014:190976. doi:10.1155/2014/190976
44. Chongtham A, Bornemann DJ, Barbaro BA, et al. Effects of flanking sequences and cellular context on subcellular behavior and pathology of mutant HTT. *Hum Mol Genet*. 2020;29(4):674-688. doi:10.1093/hmg/ddaa001
45. Vieweg S, Ansaloni A, Wang ZM, Warner JB, Lashuel HA. An intein-based strategy for the production of tag-free huntingtin exon 1 proteins enables new insights into the polyglutamine dependence of Httex1 aggregation and fibril formation. *J Biol Chem*. 2016;291(23):12074-12086. doi:10.1074/jbc.M116.713982
46. Azizyan RA, Garro A, Radkova Z, et al. Establishment of Constraints on Amyloid Formation Imposed by Steric Exclusion of Globular Domains. *J Mol Biol*. 2018;430(20):3835-3846. doi:10.1016/j.jmb.2018.05.038
47. Matsumoto G, Kim S, Morimoto RI. Huntingtin and mutant SOD1 form aggregate structures with distinct molecular properties in human cells. *J Biol Chem*. 2006;281(7):4477-4485. doi:10.1074/jbc.M509201200
48. Qin Z, Wang Y, Sapp E, et al. Huntingtin Bodies Sequester Vesicle-Associated Proteins by a Polyproline-Dependent Interaction. *J Neurosci*. 2004;24(1):269-281. doi:10.1523/JNEUROSCI.1409-03.2004
49. Suopanki J, Götz C, Lutsch G, et al. Interaction of huntingtin fragments with brain membranes - Clues to early dysfunction in Huntington's disease. *J Neurochem*. 2006;96(3):870-884. doi:10.1111/j.1471-4159.2005.03620.x
50. Hackam AS, Hodgson JG, Singaraja R, et al. Huntington ' s Disease in Cell Culture and in Transgenic Mice Expressing Mutant Huntingtin Evidence for both the nucleus and cytoplasm as subcellular sites of pathogenesis in Huntington ' s disease in cell culture and in transgenic mice expressing mutant. *Philos Trans R Soc B Biol Sci*. 2019;354(1386):1047-1055.
51. Sapp E, Schwarz C, Chase K, et al. Huntingtin localization in brains of normal and Huntington's disease patients. *Ann Neurol*. 1997;42(4):604-612. doi:10.1002/ana.410420411
52. DiFiglia M, Sapp E, Chase K, et al. Huntingtin is a cytoplasmic protein associated with vesicles in human and rat brain neurons. *Neuron*. 1995;14(5):1075-1081. doi:10.1016/0896-6273(95)90346-1
53. Sahoo B, Singer D, Kodali R, Zuchner T, Wetzel R. Aggregation behavior of chemically synthesized, full-length huntingtin exon1. *Biochemistry*. 2014;53(24):3897-3907. doi:10.1021/bi500300c
54. Aiken CT, Steffan JS, Guerrero CM, et al. Phosphorylation of threonine 3: Implications

for huntingtin aggregation and neurotoxicity. *J Biol Chem*. 2009;284(43):29427-29436. doi:10.1074/jbc.M109.013193
55. Michalek M, Salnikov ES, Werten S, Bechinger B. Membrane interactions of the amphipathic amino terminus of huntingtin. *Biochemistry*. 2013;52(5):847-858. doi:10.1021/bi301325q
56. Burke KA, Kauffman KJ, Umbaugh CS, Frey SL, Legleiter J. The interaction of polyglutamine peptides with lipid membranes is regulated by flanking sequences associated with huntingtin. *J Biol Chem*. 2013;288(21):14993-15005. doi:10.1074/jbc.M112.446237
57. Chaibva M, Gao X, Jain P, Campbell WA, Frey SL, Legleiter J. Sphingomyelin and GM1 Influence Huntingtin Binding to, Disruption of, and Aggregation on Lipid Membranes. *ACS Omega*. 2017;3(1):273-285. doi:10.1021/acsomega.7b01472
58. Boatz JC, Piretra T, Lasorsa A, Matlahov I, Conway JF, Patrick C. A. van der Wel. Protofilament structure and supramolecular polymorphism of aggregated mutant huntingtin exon 1. *J Mol Biol*. 2020;432(16):4722-4744. doi:10.1016/j.matdes.2019.108334
59. Di Pardo A, Monyror J, Morales LC, et al. Mutant huntingtin interacts with the sterol regulatory element-binding proteins and impairs their nuclear import. *Hum Mol Genet*. 2020;29(3):418-431. doi:10.1093/hmg/ddz298
60. Di Pardo A, Maglione V. The S1P Axis: New Exciting Route for Treating Huntington's Disease. *Trends Pharmacol Sci*. 2018;39(5):468-480. doi:10.1016/j.tips.2018.02.009
61. Valenza M, Rigamonti D, Goffredo D, et al. Dysfunction of the cholesterol biosynthetic pathway in Huntington's disease. *J Neurosci*. 2005;25(43):9932-9939. doi:10.1523/JNEUROSCI.3355-05.2005
62. Del Toro D, Xifró X, Pol A, et al. Altered cholesterol homeostasis contributes to enhanced excitotoxicity in Huntington's disease. *J Neurochem*. 2010;115(1):153-167. doi:10.1111/j.1471-4159.2010.06912.x
63. Labbadia J, Morimoto RI. Huntington's disease: Underlying molecular mechanisms and emerging concepts. *Trends Biochem Sci*. 2013;38(8):378-385. doi:10.1016/j.tibs.2013.05.003
64. Schipper-Krom S, Juenemann K, Jansen AH, et al. Dynamic recruitment of active proteasomes into polyglutamine initiated inclusion bodies. *FEBS Lett*. 2014;588(1):151-159. doi:10.1016/j.febslet.2013.11.023
65. Huang ZN, Her LS. The Ubiquitin Receptor ADRM1 Modulates HAP40-Induced Proteasome Activity. *Mol Neurobiol*. 2017;54(9):7382-7400. doi:10.1007/s12035-016-0247-y
66. Juenemann K, Jansen AHP, van Riel L, et al. Dynamic recruitment of ubiquitin to mutant huntingtin inclusion bodies. *Sci Rep*. 2018;8(1):1405. doi:10.1038/s41598-018-19538-0
67. Hipp MS, Patel CN, Bersuker K, et al. Indirect inhibition of 26S proteasome activity in a cellular model of Huntington's disease. *J Cell Biol*. 2012;196(5):573-587. doi:10.1083/jcb.201110093
68. Bennett EJ, Shaler TA, Woodman B, et al. Global changes to the ubiquitin system in Huntington's disease. *Nature*. 2007;448(7154):704-708. doi:10.1038/nature06022
69. Schipper-Krom S, Juenemann K, Reits EAJ. The ubiquitin-proteasome system in huntington's disease: Are proteasomes impaired, initiators of disease, or coming to the rescue? *Biochem Res Int*. 2012;2012:837015. doi:10.1155/2012/837015
70. Bansal M, Moharir SC, Swarup G. Autophagy receptor optineurin promotes autophagosome formation by potentiating LC3-II production and phagophore maturation. *Commun Integr Biol*. 2018;11(2):1-4. doi:10.1080/19420889.2018.1467189
71. N'Diaye EN, Debnath J, Brown EJ. Ubiquilins accelerate autophagosome maturation and promote cell survival during nutrient starvation. *Autophagy*. 2009;5(4):573-575. doi:10.4161/auto.5.4.8312
72. Baker B, Geng S, Chen K, et al. Alteration of lysosome fusion and low-grade

inflammation mediated by super-low-dose endotoxin. *J Biol Chem*. 2015;290(10):6670-6678. doi:10.1074/jbc.M114.611442
73. Lu K, Psakhye I, Jentsch S. Autophagic clearance of PolyQ proteins mediated by ubiquitin-Atg8 adaptors of the conserved CUET protein family. *Cell*. 2014;158(3):549-563. doi:10.1016/j.cell.2014.05.048
74. Oguro A, Kubota H, Shimizu M, Ishiura S, Atomi Y. Protective role of the ubiquitin binding protein Tollip against the toxicity of polyglutamine-expansion proteins. *Neurosci Lett*. 2011;503(3):234-239. doi:10.1016/j.neulet.2011.08.043
75. Shimizu M, Oguro-Ando A, Ohoto-Fujita E, Atomi Y. *Toll-Interacting Protein Pathway: Degradation of an Ubiquitin-Binding Protein*. Vol 534. 1st ed. Elsevier Inc.; 2014. doi:10.1016/B978-0-12-397926-1.00018-4
76. Shen WC, Li HY, Chen GC, Chern Y, Tu PH. Mutations in the ubiquitin-binding domain of OPTN/optineurin interfere with autophagy- mediated degradation of misfolded proteins by a dominant-negative mechanism. *Autophagy*. 2015;11(4):685-700. doi:10.4161/auto.36098
77. Korac J, Schaeffer V, Kovacevic I, et al. Ubiquitin-independent function of optineurin in autophagic clearance of protein aggregates. *J Cell Sci*. 2013;126(2):580-592. doi:10.1242/jcs.114926
78. Schwab C, Yu S, McGeer EG, McGeer PL. Optineurin in Huntington's disease intranuclear inclusions. *Neurosci Lett*. 2012;506(1):149-154. doi:10.1016/j.neulet.2011.10.070
79. Maruyama H, Kawakami H. Optineurin and amyotrophic lateral sclerosis. *Geriatr Gerontol Int*. 2013;13(3):528-532. doi:10.1111/ggi.12022
80. Deng Z, Purtell K, Lachance V, Wold MS, Chen S, Yue Z. Autophagy Receptors and Neurodegenerative Diseases. *Trends Cell Biol*. 2017;27(7):491-504. doi:10.1016/j.tcb.2017.01.001
81. Suhr ST, Senut MC, Whitelegge JP, Faull KF, Cuizon DB, Gage FH. Identities of sequestered proteins in aggregates from cells with induced polyglutamine expression. *J Cell Biol*. 2001;153(2):283-294. doi:10.1083/jcb.153.2.283
82. Kazantsev A, Preisinger E, Dranovsky A, Goldgaber D, Housman D. Insoluble detergent-resistant aggregates form between pathological and nonpathological lengths of polyglutamine in mammalian cells. *Proc Natl Acad Sci U S A*. 1999;96(20):11404-11409. doi:10.1073/pnas.96.20.11404
83. Scior A, Buntru A, Arnsburg K, et al. Complete suppression of Htt fibrilization and disaggregation of Htt fibrils by a trimeric chaperone complex. *EMBO J*. 2018;37(2):282-299. doi:10.15252/embj.201797212
84. Hjerpe R, Bett JS, Keuss MJ, et al. UBQLN2 Mediates Autophagy-Independent Protein Aggregate Clearance by the Proteasome. *Cell*. 2016;166(4):935-949. doi:10.1016/j.cell.2016.07.001
85. Culver BP, DeClercq J, Dolgalev I, et al. Huntington's Disease Protein Huntingtin Associates with its own mRNA. *J Huntingtons Dis*. 2016;5(1):39-51. doi:10.3233/JHD-150177
86. Bowles KR, Stone T, Holmans P, Allen ND, Dunnett SB, Jones L. SMAD transcription factors are altered in cell models of HD and regulate HTT expression. *Cell Signal*. 2017;31:1-14. doi:10.1016/j.cellsig.2016.12.005
87. Feyeux M, Bourgois-Rocha F, Redfern A, et al. Early transcriptional changes linked to naturally occurring Huntington's disease mutations in neural derivatives of human embryonic stem cells. *Hum Mol Genet*. 2012;21(17):3883-3895. doi:10.1093/hmg/dds216
88. Borovecki F, Lovrecic L, Zhou J, et al. Genome-wide expression profiling of human blood reveals biomarkers for Huntington's disease. *Proc Natl Acad Sci U S A*. 2005;102(31):11023-11028. doi:10.1073/pnas.0504921102
89. Runne H, Kuhn A, Wild EJ, et al. Analysis of potential transcriptomic biomarkers for Huntington's disease in peripheral blood. *Proc Natl Acad Sci U S A*. 2007;104(36):14424-14429. doi:10.1073/pnas.0703652104

90. Mastrokolias A, Ariyurek Y, Goeman JJ, et al. Huntington's disease biomarker progression profile identified by transcriptome sequencing in peripheral blood. *Eur J Hum Genet*. 2015;23(10):1349-1356. doi:10.1038/ejhg.2014.281
91. Croce KR, Yamamoto A. A role for autophagy in Huntington's disease. *Neurobiol Dis*. 2019;122:16-22. doi:10.1016/j.nbd.2018.08.010
92. Snapp EL, Hegde RS, Francolini M, et al. Formation of stacked ER cisternae by low affinity protein interactions. *J Cell Biol*. 2003;163(2):257-269. doi:10.1083/jcb.200306020
93. McCaughey J, Miller VJ, Stevenson NL, et al. TFG Promotes Organization of Transitional ER and Efficient Collagen Secretion. *Cell Rep*. 2016;15(8):1648-1659. doi:10.1016/j.celrep.2016.04.062
94. Witte K, Schuh AL, Hegermann J, et al. TFG-1 function in protein secretion and oncogenesis. *Nat Cell Biol*. 2011;13(5):550-558. doi:10.1038/ncb2225
95. Tellez-Nagel I, Johnson AB, Terry RD. Studies on brain biopsies of patients with Huntington's chorea. *J Neuropathol Exp Neurol*. 1974;33(2):308-332.
96. Gasset-Rosa F, Chillon-Marinas C, Goginashvili A, et al. Polyglutamine-Expanded Huntingtin Exacerbates Age-Related Disruption of Nuclear Integrity and Nucleocytoplasmic Transport. *Neuron*. 2017;94(1):48-57.e4. doi:10.1016/j.neuron.2017.03.027
97. Maiuri T, Hung CLK, Suart C, et al. DNA Repair in Huntington's Disease and Spinocerebellar Ataxias: Somatic Instability and Alternative Hypotheses. *J Huntingtons Dis*. 2021;10(1):165-173. doi:10.3233/JHD-200414
98. Ratovitski T, Chighladze E, Arbez N, et al. Huntingtin protein interactions altered by polyglutamine expansion as determined by quantitative proteomic analysis. *Cell Cycle*. 2012;11(10):2006-2021. doi:10.4161/cc.20423
99. Sap KA, Guler AT, Bezstarosti K, et al. Global proteome and ubiquitinome changes in the soluble and insoluble fractions of Q175 huntington mice brains. *Mol Cell Proteomics*. 2019;18(9):1705-1720. doi:10.1074/mcp.RA119.001486
100. Hosp F, Gutiérrez-Ángel S, Schaefer MH, et al. Spatiotemporal Proteomic Profiling of Huntington's Disease Inclusions Reveals Widespread Loss of Protein Function. *Cell Rep*. 2017;21(8):2291-2303. doi:10.1016/j.celrep.2017.10.097
101. Hodges A, Hughes G, Brooks S, et al. Brain gene expression correlates with changes in behavior in the R6/1 mouse model of Huntington's disease. *Genes, Brain Behav*. 2008;7(3):288-299. doi:10.1111/j.1601-183X.2007.00350.x
102. Christodoulou CC, Zachariou M, Tomazou M, et al. Investigating the transition of pre-symptomatic to symptomatic huntington's disease status based on omics data. *Int J Mol Sci*. 2020;21(19):1-26. doi:10.3390/ijms21197414
103. Safren N, Chang L, Dziki KM, Monteiro MJ. Signature changes in ubiquilin expression in the R6/2 mouse model of Huntington's disease. *Brain Res*. 2015;1597:37-46. doi:10.1016/j.brainres.2014.12.008
104. Safren N, El Ayadi A, Chang L, et al. Ubiquilin-1 overexpression increases the lifespan and delays accumulation of huntingtin aggregates in the R6/2 mouse model of huntington's disease. *PLoS One*. 2014;9(1):1-13. doi:10.1371/journal.pone.0087513
105. Sticker A, Goeminne L, Martens L, Clement L. Robust summarization and inference in proteome-wide label-free quantification. *Mol Cell Proteomics*. 2020;19(7):1209-1219. doi:10.1074/mcp.RA119.001624
106. Wear MP, Kryndushkin D, O'Meally R, et al. Proteins with intrinsically disordered domains are preferentially recruited to polyglutamine aggregates. *PLoS One*. 2015;10(8):1-27. doi:10.1371/journal.pone.0136362
107. Mizukami K, Abrahamson EE, Mi Z, et al. Immunohistochemical analysis of ubiquilin-1 in the human hippocampus: Association with neurofibrillary tangle pathology. *Neuropathology*. 2014;34(1):11-18. doi:10.1111/neup.12055
108. Dil Kuazi A, Kito K, Abe Y, Shin RW, Kamitani T, Ueda N. NEDD8 protein is involved in ubiquitinated inclusion bodies. *J Pathol*. 2003;199(2):259-266. doi:10.1002/path.1283

109. Mori F, Nishie M, Piao YS, et al. Accumulation of NEDD8 in neuronal and glial inclusions of neurodegenerative disorders. *Neuropathol Appl Neurobiol*. 2005;31(1):53-61. doi:10.1111/j.1365-2990.2004.00603.x
110. Maghames CM, Lobato-Gil S, Perrin A, et al. NEDDylation promotes nuclear protein aggregation and protects the Ubiquitin Proteasome System upon proteotoxic stress. *Nat Commun*. 2018;9(1):1-17. doi:10.1038/s41467-018-06365-0
111. Ray PD, Huang B-W, Tsuji Y. Reactive oxygen species (ROS) homeostasis and redox regulation in cellular signaling. *Cell Signal*. 2012;24(5):981-990. doi:10.1016/j.cellsig.2012.01.008
112. Chang DTW, Rintoul GL, Pandipati S, Reynolds IJ. Mutant huntingtin aggregates impair mitochondrial movement and trafficking in cortical neurons. *Neurobiol Dis*. 2006;22(2):388-400. doi:10.1016/j.nbd.2005.12.007
113. Bossy-Wetzel E, Petrilli A, Knott AB. Mutant Huntintin and Mitochondrial Dysfunction. *Trends Neurosci*. 2008;31(12):609-616. doi:10.1016/j.tins.2008.09.004.MUTANT
114. A. Crotti, Benner C, Kerman B, et al. Mutant Huntingtin promotes autonomous microglia activation via myeloid lineage-determining factors. *Nat Neurosci*. 2014;17(4):513-521. doi:10.1038/jid.2014.371
115. Manczak M, Hemachandra Reddy P. Mitochondrial division inhibitor 1 protects against mutant huntingtin-induced abnormal mitochondrial dynamics and neuronal damage in Huntington's disease. *Hum Mol Genet*. 2015;24(25):7308-7325. doi:10.1093/hmg/ddv429
116. Yin X, Manczak M, Reddy PH. Mitochondria-targeted molecules MitoQ and SS31 reduce mutant huntingtin-induced mitochondrial toxicity and synaptic damage in Huntington's disease. *Hum Mol Genet*. 2016;25(9):1739-1753. doi:10.1093/hmg/ddw045
117. Ugalde CL, Annesley SJ, Gordon SE, et al. Misfolded α-synuclein causes hyperactive respiration without functional deficit in live neuroblastoma cells. *DMM Dis Model Mech*. 2020;13(1):dmm040899. doi:10.1242/dmm.040899
118. Horn A, Raavicharla S, Shah S, Cox D, Jaiswal JK. Mitochondrial fragmentation enables localized signaling required for cell repair. *J Cell Biol*. 2020;219(5):e201909154. doi:10.1083/jcb.201909154
119. Forno LS, Norville RL. Ultrastructure of Lewy bodies in the stellate ganglion. *Acta Neuropathol*. 1976;34(3):183-197. doi:10.1007/BF00688674
120. Gai WP, Yuan HX, Li XQ, Power JTH, Blumbergs PC, Jensen PH. In situ and in vitro study of colocalization and segregation of α-synuclein, ubiquitin, and lipids in Lewy bodies. *Exp Neurol*. 2000;166(2):324-333. doi:10.1006/exnr.2000.7527
121. Shahmoradian SH, Lewis AJ, Genoud C, et al. Lewy pathology in Parkinson's disease consists of crowded organelles and lipid membranes. *Nat Neurosci*. 2019;22(7):1099-1109. doi:10.1038/s41593-019-0423-2
122. Mahul-Mellier A-L, Burtscher J, Maharjan N, et al. The process of Lewy body formation, rather than simply alpha-synuclein fibrillization, is the major driver of neurodegeneration. *Proc Natl Acad Sci*. 2020;117(9):4971-4982. doi:10.1073/1913904117
123. DiFiglia M, Sapp ME, Chase KO, et al. Aggregation of Huntingtin in Neuronal Intranuclear Inclusions and Dystrophic Neurites in Brain. *Science (80-)*. 1997;277(5334):1990-1993. doi:10.1126/science.277.5334.1990
124. Choo YS, Johnson GVW, MacDonald M, Detloff PJ, Lesort M. Mutant huntingtin directly increases susceptibility of mitochondria to the calcium-induced permeability transition and cytochrome c release. *Hum Mol Genet*. 2004;13(14):1407-1420. doi:10.1093/hmg/ddh162
125. Song W, Chen J, Petrilli A, et al. Mutant huntingtin binds the mitochondrial fission GTPase dynamin-related protein-1 and increases its enzymatic activity. *Nat Med*. 2011;17(3):377-383. doi:10.1038/nm.2313
126. Brennan WA, Bird ED, Aprille JR. Regional Mitochondrial Respiratory Activity in Huntington's Disease Brain. *J Neurochem*. 1985;44(6):1948-1950. doi:10.1111/j.1471-

4159.1985.tb07192.x
127. Gu M, Gash MT, Mann VM, Javoy-Agid F, Cooper JM, Schapira AHV. Mitochondrial defect in Huntington's disease caudate nucleus. *Ann Neurol*. 1996;39(3):385-389. doi:10.1002/ana.410390317
128. Browne SE, Bowling AC, MacGarvey U, et al. Oxidative damage and metabolic dysfunction in huntington's disease: Selective vulnerability of the basal ganglia. *Ann Neurol*. 1997;41(5):646-653. doi:10.1002/ana.410410514
129. Kegel KB, Kim M, Sapp E, et al. Huntingtin expression stimulates endosomal-lysosomal activity, endosome tubulation, and autophagy. *J Neurosci*. 2000;20(19):7268-7278. doi:10.1523/jneurosci.20-19-07268.2000
130. Stephens DJ. De novo formation, fusion and fission of mammalian COPII-coated endoplasmic reticulum exit sites. *EMBO Rep*. 2003;4(2):210-217. doi:10.1038/sj.embor.embor736
131. Farhan H, Weiss M, Tani K, Kaufman RJ, Hauri HP. Adaptation of endoplasmic reticulum exit sites to acute and chronic increases in cargo load. *EMBO J*. 2008;27(15):2043-2054. doi:10.1038/emboj.2008.136
132. Vidal R, Caballero B, Couve A, Hetz C. Converging pathways in the occurrence of endoplasmic reticulum (ER) stress in Huntington's disease. *Curr Mol Med*. 2011;11(1):1-12. doi:10.2174/156652411794474419
133. Jiang R, Diaz-Castro B, Looger LL, Khakh BS. Dysfunctional Calcium and Glutamate Signaling in Striatal Astrocytes from Huntington's Disease Model Mice. *J Neurosci*. 2016;36(12):3453-3470. doi:10.1523/JNEUROSCI.3693-15.2016
134. Lee KS, Huh S, Lee S, et al. Altered ER-mitochondria contact impacts mitochondria calcium homeostasis and contributes to neurodegeneration in vivo in disease models. *Proc Natl Acad Sci U S A*. 2018;115(38):E8844-E8853. doi:10.1073/pnas.1815900115
135. El-Daher M-T, Hangen E, Bruyere J, et al. Huntingtin proteolysis releases non-polyQ fragments that cause toxicity through dynamin 1 dysregulation. *EMBO J*. 2015;34(17):2255-2271. doi:10.15252/embj.201490808
136. Leitman J, Ulrich Hartl F, Lederkremer GZ. Soluble forms of polyQ-expanded huntingtin rather than large aggregates cause endoplasmic reticulum stress. *Nat Commun*. 2013;4:2753. doi:10.1038/ncomms3753
137. Higo T, Hamada K, Hisatsune C, et al. Mechanism of ER Stress-Induced Brain Damage by IP3 Receptor. *Neuron*. 2010;68(5):865-878. doi:10.1016/j.neuron.2010.11.010
138. Romero-grimaldi C, Moreno-lo B. Age-Dependent Effect of Nitric Oxide on Subventricular Zone and Olfactory Bulb. *J Comp Neurol*. 2008;506(2):339-346. doi:10.1002/cne
139. Tagawa K, Hoshino M, Okuda T, et al. Distinct aggregation and cell death patterns among different types of primary neurons induced by mutant huntingtin protein. *J Neurochem*. 2004;89(4):974-987. doi:10.1111/j.1471-4159.2004.02372.x
140. Peters MF, Nucifora FC, Kushi J, et al. Nuclear targeting of mutant huntingtin increases toxicity. *Mol Cell Neurosci*. 1999;14(2):121-128. doi:10.1006/mcne.1999.0773
141. Benn CL, Landles C, Li H, et al. Contribution of nuclear and extranuclear polyQ to neurological phenotypes in mouse models of Huntington's disease. *Hum Mol Genet*. 2005;14(20):3065-3078. doi:10.1093/hmg/ddi340
142. Greiner ER, Yang XW. Huntington's disease: Flipping a switch on huntingtin. *Nat Chem Biol*. 2011;7(7):412-414. doi:10.1038/nchembio.604
143. Deguire SM, Ruggeri FS, Fares M, et al. N-terminal Huntingtin (Htt) phosphorylation is a molecular switch regulating Htt aggregation, helical conformation, internalization, and nuclear targeting. *J Biol Chem*. 2018;(12). doi:10.1074/jbc.RA118.004621
144. Li L, Liu H, Dong P, et al. Real-time imaging of Huntingtin aggregates diverting target search and gene transcription. *Elife*. 2016;5:e17056. doi:10.7554/eLife.17056.001
145. Posey AE, Ruff KM, Harmon TS, et al. Profilin reduces aggregation and phase separation of huntingtin N-terminal fragments by preferentially binding to soluble

monomers and oligomers. *J Biol Chem*. 2018;293(10):3734-3746. doi:10.1074/jbc.RA117.000357
146. Poirier MA, Li H, Macosko J, Cai S, Amzel M, Ross CA. Huntingtin spheroids and protofibrils as precursors in polyglutamine fibrilization. *J Biol Chem*. 2002;277(43):41032-41037. doi:10.1074/jbc.M205809200
147. Liu KY, Shyu YC, Barbaro BA, et al. Disruption of the nuclear membrane by perinuclear inclusions of mutant huntingtin causes cell-cycle re-entry and striatal cell death in mouse and cell models of Huntington's disease. *Hum Mol Genet*. 2015;24(6):1602-1616. doi:10.1093/hmg/ddu574
148. Firdaus WJJ, Wyttenbach A, Giuliano P, Kretz-Remy C, Currie RW, Arrigo AP. Huntingtin inclusion bodies are iron-dependent centers of oxidative events. *FEBS J*. 2006;273(23):5428-5441. doi:10.1111/j.1742-4658.2006.05537.x
149. Miller J, Arrasate M, Shaby BA, Mitra S, Masliah E, Finkbeiner S. Quantitative relationships between huntingtin levels, polyglutamine length, inclusion body formation, and neuronal death provide novel insight into huntington's disease molecular pathogenesis. *J Neurosci*. 2010;30(31):10541-10550. doi:10.1523/JNEUROSCI.0146-10.2010
150. Kolla R, Gopinath P, Ricci J, Reif A, Rostami I, Lashuel HA. A New Chemoenzymatic Semisynthetic Approach Provides Insight into the Role of Phosphorylation beyond Exon1 of Huntingtin and Reveals N-Terminal Fragment Length-Dependent Distinct Mechanisms of Aggregation. *J Am Chem Soc*. 2021;143(26):9798-9812. doi:10.1021/jacs.1c03108

Author contributions

H.A.L conceived and supervised the study. H.A.L, N.R and A.L.M.M designed all the experiments and wrote the paper. N.R performed and analyzed the confocal imaging, the electron microscopy and the 3D imaging reconstruction, quantitative proteomic experiments and the biochemistry experiments. A.L.M.M performed and analyzed the CLEM experiment and analyzed the proteomic data. N.M designed and analyzed the proteomic data. J.B designed, performed, and analyzed the high-resolution respirometry experiments. A.P helped to perform and analyze the confocal imaging experiments. M.C prepared the samples for CLEM and acquired the EM and ET images. G.K supervised the EM-related experiments and 3D imaging reconstruction and contributed to the interpretation of the data. S.N generated, annotated and analyzed the tomograms. J.H. analyzed the proteomic data. V.R and H.F designed, performed, and analyzed the experiments related to ER. All authors reviewed and contributed to the writing.

Competing interests statement

The authors declare no competing financial interests in association with this manuscript.

Acknowledgments

This work was supported by funding from the Ecole Polytechnique Fédérale de Lausanne (EPFL) and the CHDI Foundation (H.A.L, N.R, A.L.M, N.M, J.B and A.P). We thank Dr. Arne Seitz and the staff at the Bio-imaging Core Facility (BioP, EPFL) for their technical support and valuable discussions. We are grateful to the Proteomics Core Facility (EPFL): Dr. Diego Chiappe, Dr. Romain Hamelin and Dr. Florence Armand for their guidance, helpful discussions and support with the proteomic studies. We also thank Stéphanie Rosset and Anaëlle Dubois at the Bio-EM Core facility (EPFL) as well as Dr. Davide Demurtas from the CIME core facility (EPFL) for their technical support. We are grateful to the research associates in the Lashuel Lab: Driss Boudeffa, Jonathan Ricci and Yllza Jasiqi for their continuous technical assistance. We thank Lorene Aeschbach for the preparation of primary

neuronal cultures. We are grateful to Dr. Pedro Magalhães (LMNN, EPFL) for his help and guidance on the proteomic analysis as well as comments on the manuscript. We thank Dr. Andrea Caricasole (IRBM) for kindly providing the pCMV mammalian expression vector encoding for the basic Httex1 constructs. We would also like to thank Dr. Magda Zachara (UPDEPLA, EPFL) for the Bodipy staining and useful discussions. The graphical abstract, Figure 5C and Figure 10 were created with BioRender.com.

Figures

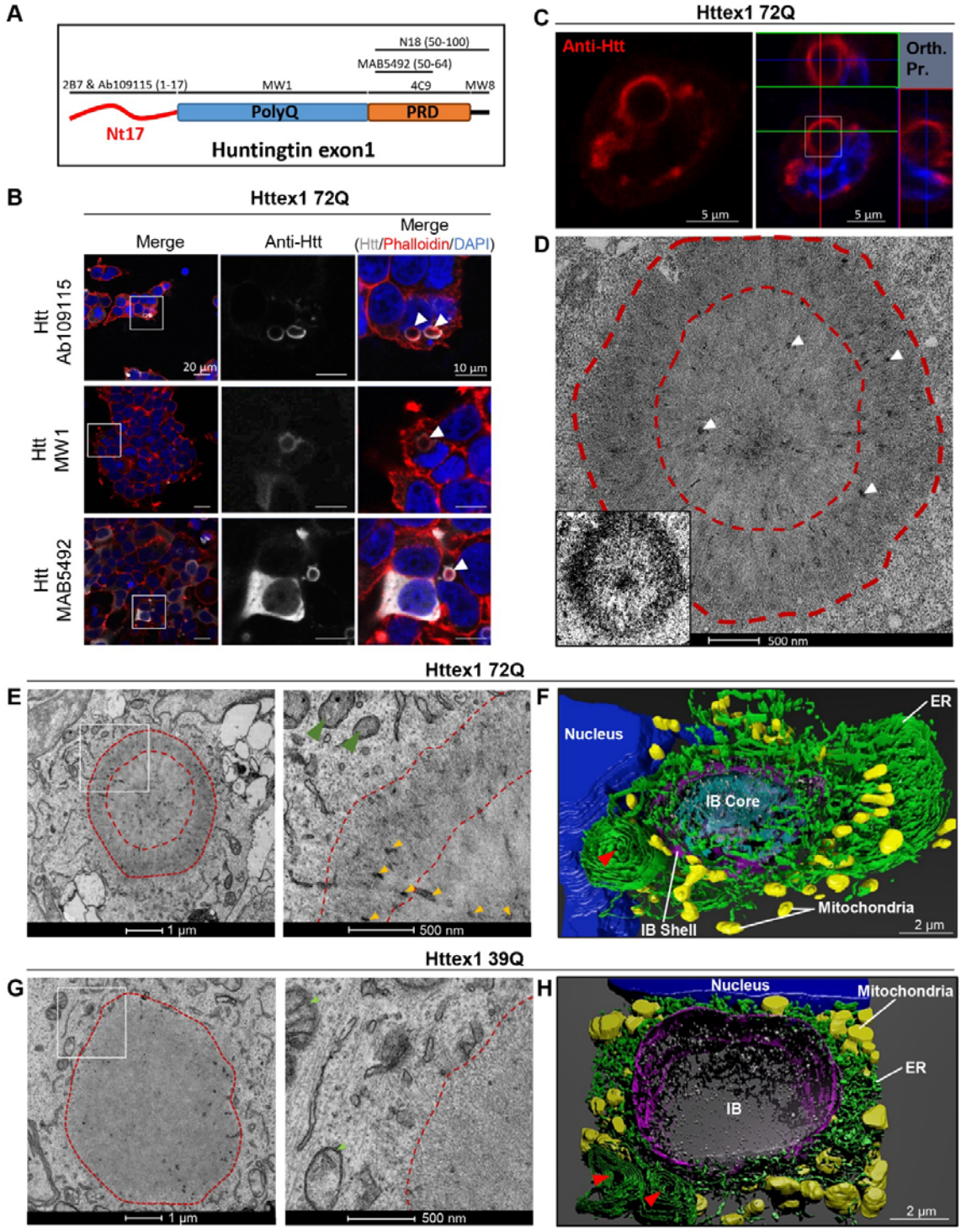

Figure 1. Confocal microscopy and CLEM revealed the ring-like structure of the Httex1 72Q inclusions formed in HEK cells. A. Epitope mapping of the Httex1 antibodies. **B.** Httex1 72Q inclusions that formed 48 h after transfection in HEK cells were detected by ICC staining combined with confocal imaging. All the Htt antibodies showed strong immunoreactivity to the periphery of the Httex1 inclusions. The nucleus was counterstained with DAPI (blue) and the F-actin with phalloidin (red). White arrows indicate the colocalization

of the F-actin with the ring-like structure of Httex1 inclusions. Scale bar = 20 µm (left-hand panels) and 10 µm (middle and right-hand panels). **C-D.** 48 h post-transfection, HEK cells were fixed, and ICC against Httex1 was performed and imaged by confocal microscopy (**C**). The selected area of the cells (white square) was then examined by EM. Orthogonal projection (Orth. Pr.), Scale bars = 5 µm. (**D**). Pieces of membranes and vesicles are indicated by the white arrowheads. A binary image (inset) was generated from the electron micrograph using a median filtering and Otsu intensity threshold, allowing for a better distinction between the core and the shell ultrastructure of the tag-free Httex1 inclusion. Scale bar = 500 nm. **E.** Representative electron micrograph of Httex1 72Q cellular inclusion and higher magnification (white square) shown in the right panel. Dashed lines delimit the aggregate and the core of the inclusion. Internalized membranous structures and the mitochondria are indicated by the orange arrowheads and the green arrowheads, respectively. Scale bar = 1 µm (left panel) and 500 nm (right panel) **F.** 3D model of Httex1 72Q cellular inclusion and surrounding organelles (top view). The Httex1 inclusion body (IB) shell is represented in purple and the IB core in cyan. ER membranes are shown in green, intra-inclusion membranous structures are displayed in white, the nucleus is shown in blue, and the mitochondria are shown in yellow. A red arrow highlights the formation of stacked ER cisternae. Scale bar = 2 µm. **G.** Representative electron micrograph of Httex1 39Q inclusion formed 48 h after transfection in HEK. The white square indicates the area shown in the right panel at higher magnification. Dashed lines delimit the inclusion. Httex1 39Q inclusions appeared less dense than the Httex1 72Q inclusions. Scale bar = 1 µm (left panel) and 500 nm (right panel). **H.** 3D model of the Httex1 39Q inclusion body (IB) is shown in purple, surrounded by mitochondria (yellow) and ER structures (green). A red arrow highlights the formation of stacked ER cisternae close to the Httex1 39Q inclusion. Intra-inclusion membranous structures are shown in white. The nucleus is highlighted in blue. Scale bar = 2 µm.

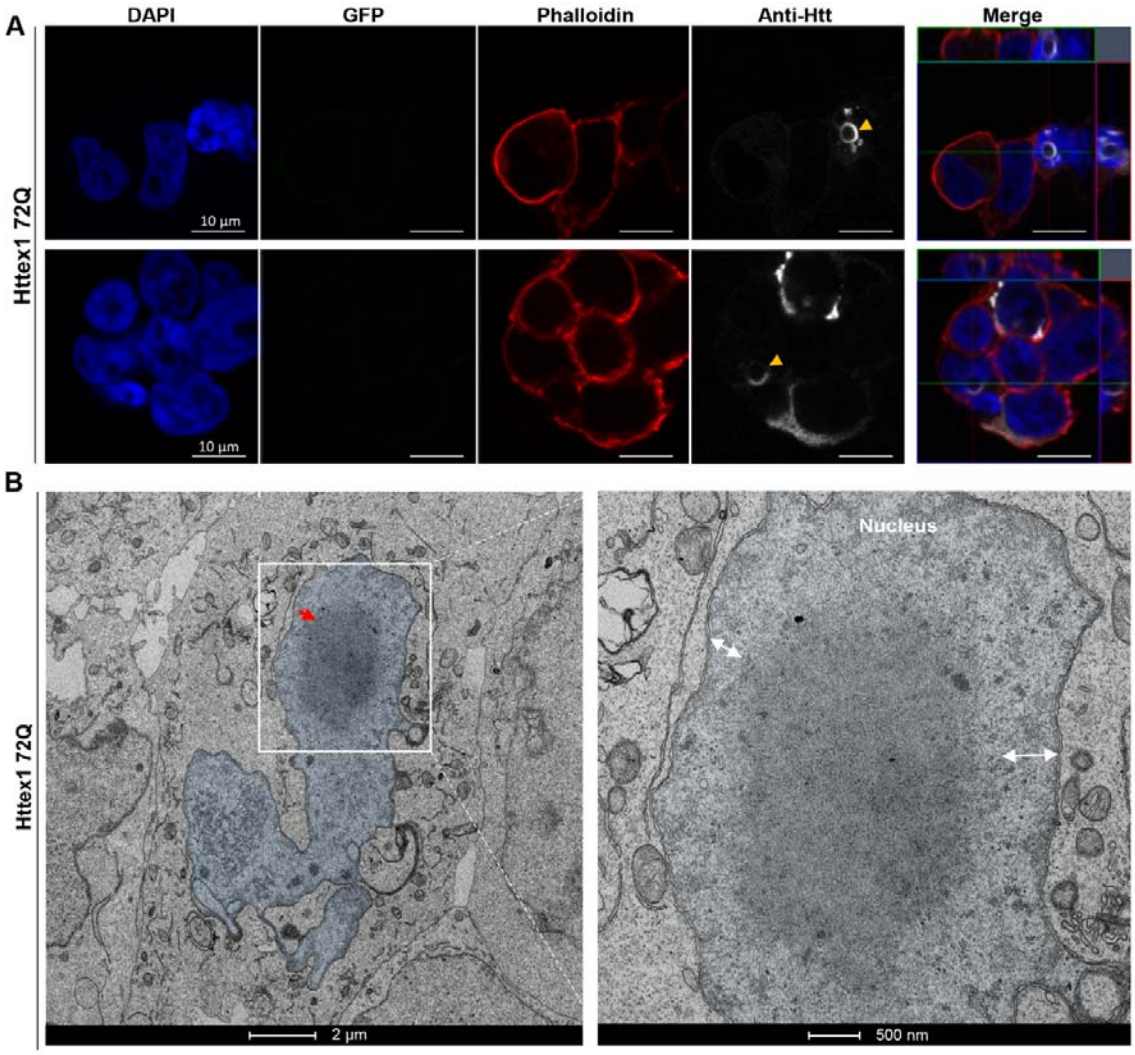

Figure 2. The nuclear inclusions formed by Httex1 72Q do not exhibit the classical core and shell organization observed for the cytosolic inclusions. A. Representative confocal images of Httex1 72Q nuclear inclusions, 48 h after transfection. Httex1 expression (grey) was detected using a specific primary antibody against the N-terminal part of Htt (amino acids 1-17; 2B7 or Ab109115). The nucleus was counterstained with DAPI (blue), and phalloidin (red) was used to stain the actin F. Httex1 nuclear inclusions are indicated by the yellow arrowheads. Scale bars = 10 µm. **B.** Electron micrograph of a representative nuclear Httex1 72Q inclusion. The white square indicates the area shown at higher magnification in the right-hand panel. The nucleus is highlighted in blue, and the double arrows indicate the distance between the nuclear inclusion and the nuclear membrane. No interaction between the nuclear inclusion and the nuclear membrane was observed. Scale bars = 2 µm (left-hand panel) and 500 nm (right-hand panel).

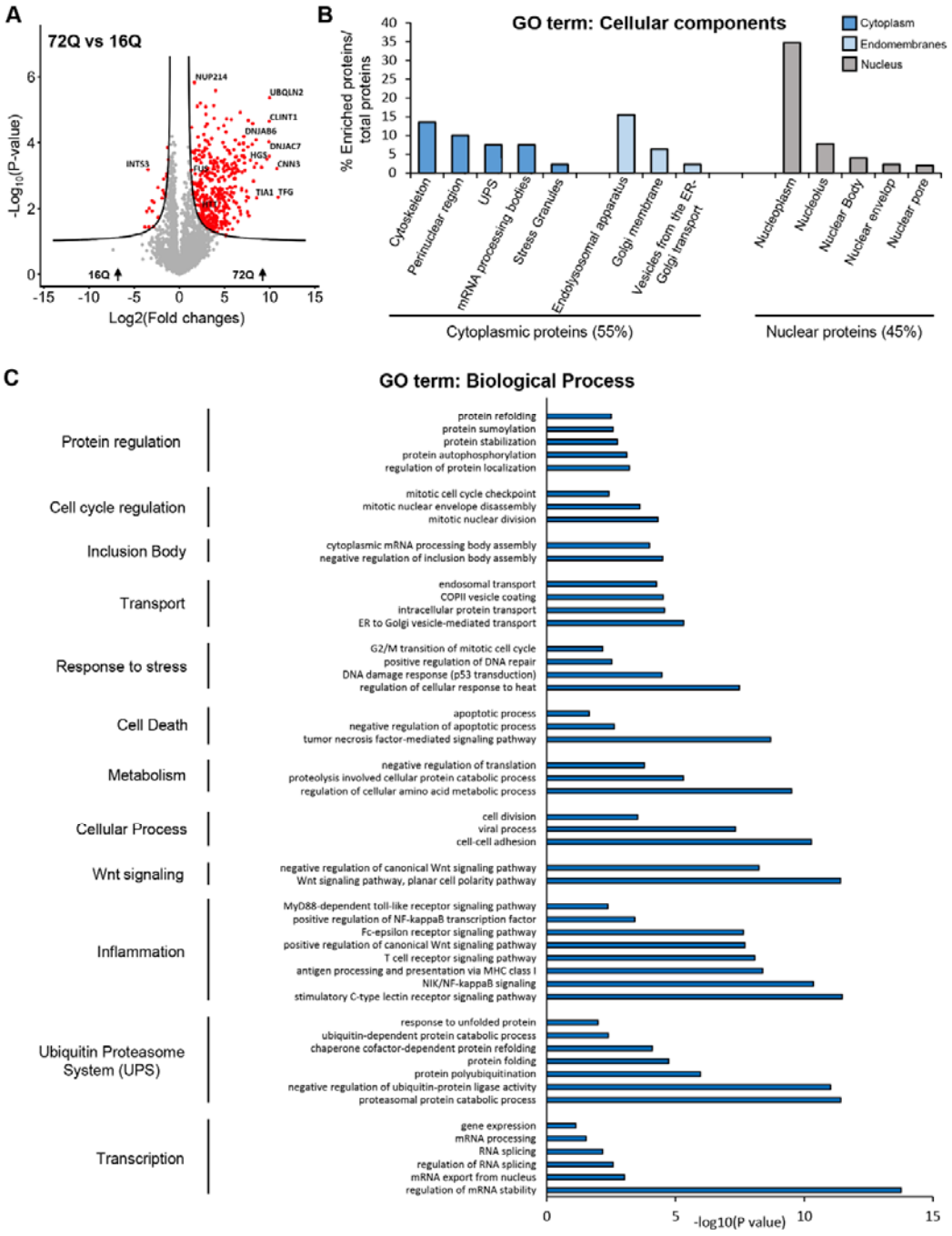

Figure 3. Proteomic analysis of the enriched protein contents found in the insoluble fraction of HEK expressing Httex1 72Q reveals protein aggregation and stress response pathways. Urea soluble proteins from HEK expressing Httex1 72Q or Httex1 16Q of 3 independent experiments were extracted 48 h after transfection and analyzed using LC-MS/MS. **A.** Identified proteins were plotted using a volcano plot. Black lines represent the threshold of significance at a false discovery rate (FDR) <0.05 and an S0 of 0.5 which were used for the subsequent analysis. **B-C**. Proteins significantly enriched in Httex1 72Q (red dots in the right part of the volcano plot) were classified by cellular component (**B**) or biological processes (**C**) using Gene Ontology (GO) term and DAVID enrichment ($-\log_{10}$(p-value) >1) analyses.

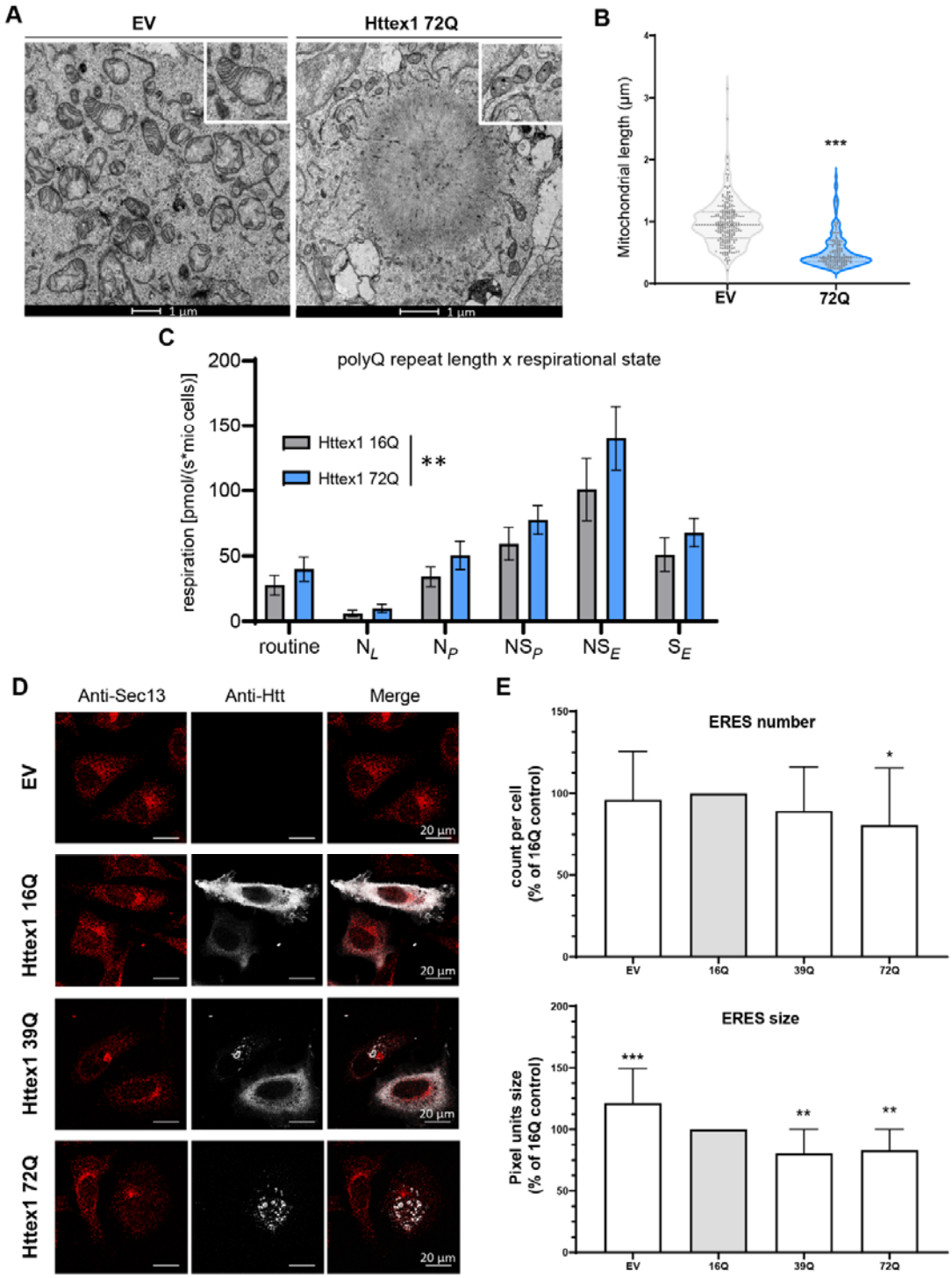

Figure 4. Formation of Httex1 72Q inclusions induces mitochondrial alterations and induces the reduction of ER-exit sites. A. Electron micrographs of mitochondria in HEK cells overexpressing empty vector (EV) or Httex1 72Q. The insets depict higher magnification of the mitochondria found at the periphery of the Httex1 72Q inclusions or representative in EV controls. Scale bars = 1 µm. **B.** Measurement of the mitochondrial length with FIJI reveals a significant reduction in the size of the mitochondrial profile located in the proximity of the inclusions. **C.** HEK cells from 4 independent experiments were gently detached for high-resolution respirometry (HRR) 48 h after transfection with indicated constructs. HRR was performed in respiration media (MIR05). After the measurements of routine respiration, cells

were chemically permeabilized by digitonin, and different respirational states were subsequently induced using a substrate-uncoupler-inhibitor titration (SUIT) protocol. Routine respiration, NADH-driven, or complex 1-linked respiration after the addition of ADP (OXPHOS state) (NP), NADH- and succinate driven, or complex 1 and 2-linked respiration in the OXPHOS state (NSP), and in the uncoupled electron transport system (ETS) capacity (NSE), as well as succinate driven, or complex 2-linked respiration in the ETS state (SE) were assessed. (B) An unpaired t-test was performed. (C) The graphs represent the mean ± SD of 4 independent experiments. (C) Two-way ANOVA showing a significant interaction between the respirational states and the polyQ repeat length. **D.** Representative confocal images of HeLa cells transfected with Httex1 16Q, 39Q, or 72Q or the empty vector (EV) as the negative control. Cells were fixed 48 h after transfection and immunostained. Httex1 was detected with the MAB5492 Htt antibody (grey), and ER exit sites were detected with Sec13 (red). Scale bars = 20 µm. **E**. ERES number and size quantification from confocal imaging was performed using FIJI. The graphs represent the mean ± SD of 3 independent experiments represented as the relative percentage of the Httex1 16Q control. ANOVA followed by a Tukey honest significant difference [HSD] post hoc test was performed. *P < 0.05, **P < 0.005, ***P < 0.001.

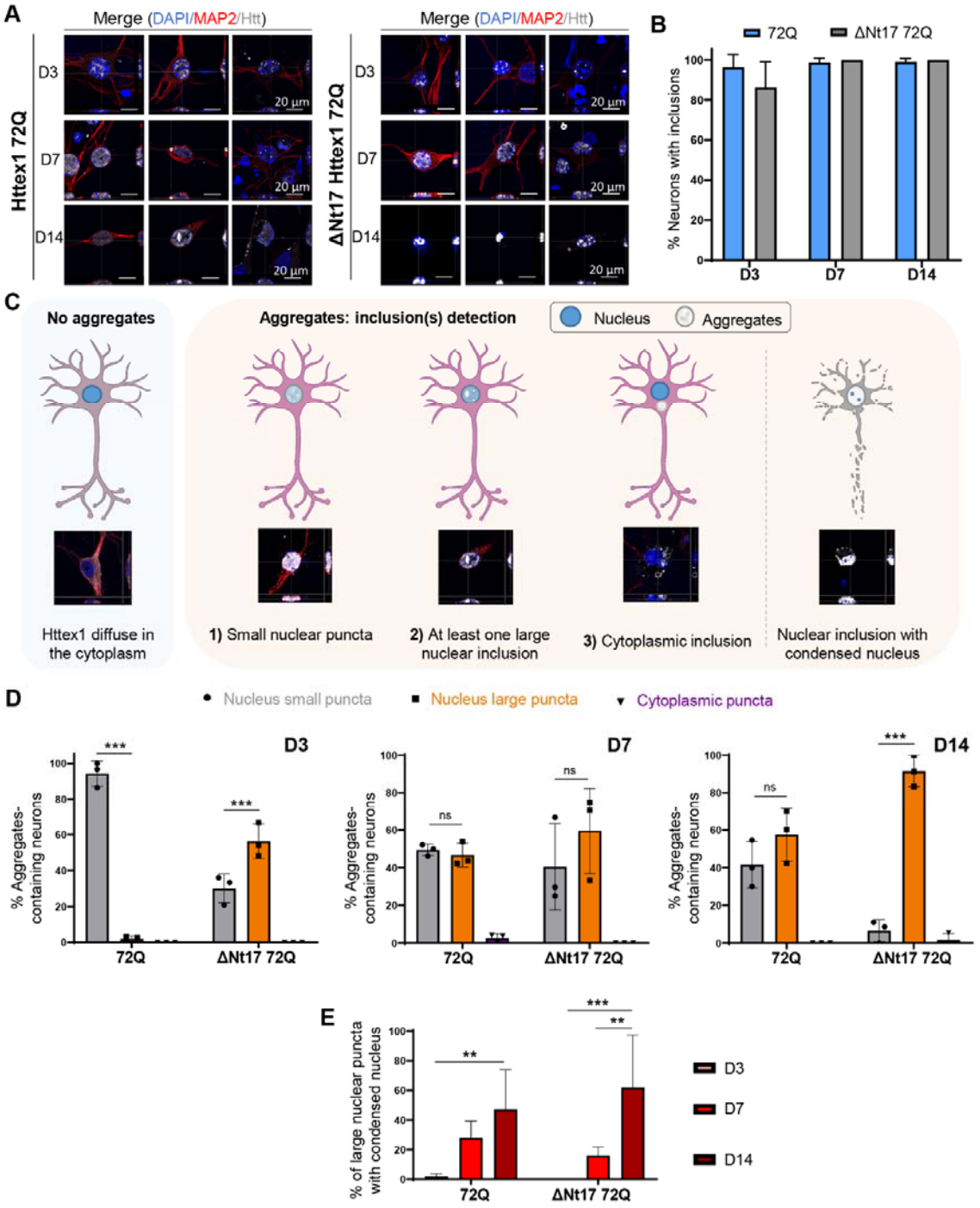

Figure 5. Confocal microscopy analysis and classification of the Httex1 inclusions formed in neurons revealed their morphological heterogeneity over time. A. Httex1 expression was detected by ICC staining combined with confocal imaging in primary cortical neurons, 3- (D3), 7- (D7) and 14- (D14) days after lentiviral transduction. Httex1 mutants were detected with the MAB5492 antibody. The nucleus was counterstained with DAPI (blue), and MAP2 was used to visualize the neurons (red). Scale bar = 20 µm. **B.** Image-based quantification of the number of neurons containing Httex1 inclusions over time. The graphs represent the mean ± SD of 3 independent experiments. **C.** Primary neurons were classified via the detection of Httex1 as diffuse or by the morphology of the detected Httex1 aggregates: 1) Small nuclear puncta; 2) at least one large nuclear inclusion, and 3)

cytoplasmic inclusion. In addition, a subclass was created for neurons containing a large nuclear inclusion associated with nuclear condensation. **D.** Image-based quantification and classification of the different morphologies of Httex1 inclusions based on the panel C. Statistical analysis: ANOVA followed by a Tukey honest significant difference [HSD] post hoc test was performed, *P < 0.05, **P < 0.005, ***P < 0.001. **E.** Image-based quantification of neurons containing a large nuclear inclusion with a nuclear condensation. Statistical analysis: Two-way ANOVA followed by a HSD post hoc test was performed, *P < 0.05, **P < 0.005, ***P < 0.001.

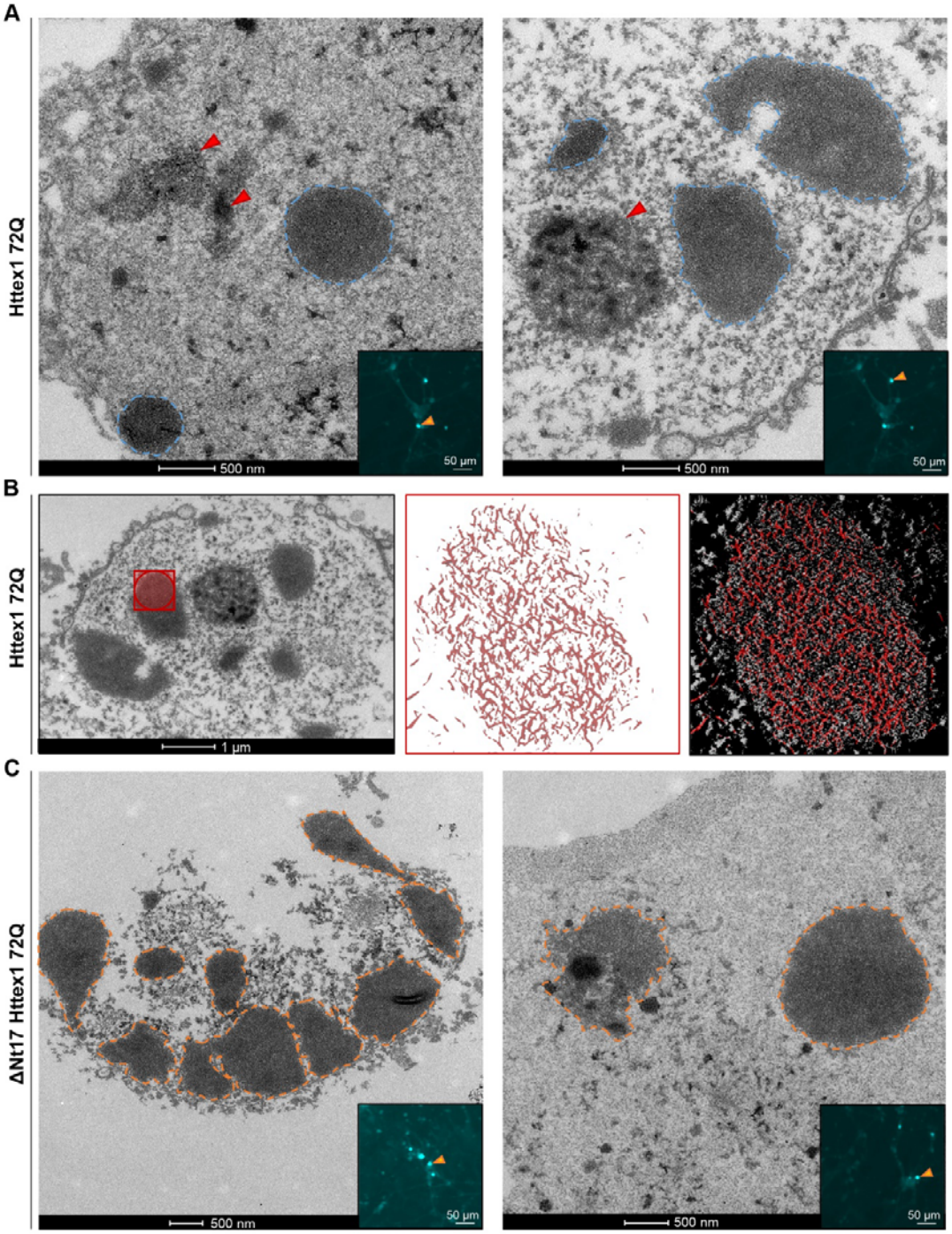

Figure 6. Ultrastructural analysis of the nuclear Httex1 72Q inclusions formed in primary cortical neurons shows granular and filamentous structures by CLEM and Tomography.

A. Representative electron micrographs of Httex1 72Q inclusions formed 7 days after lentiviral transduction in mouse cortical primary neurons. Blue dashed lines represent the inclusions, and the red arrowheads the nucleolus. Scale bar = 500 nm for the EM images and 50 µm for the fluorescent image (inset). **B.** Electron micrograph and corresponding tomogram (selected area in red) of a neuronal Httex1 72Q inclusion. Segmentation of the tomogram reveals the presence of a multitude of filaments. **C.** Representative electron micrographs of ΔNt17 Httex1 72Q inclusions formed seven days after lentiviral transduction in mouse cortical primary neurons. Orange dashed lines represent the inclusions, and the

red arrowheads the nucleolus. Scale bar = 500 nm for the EM images and 50 μm for the fluorescent image (inset).

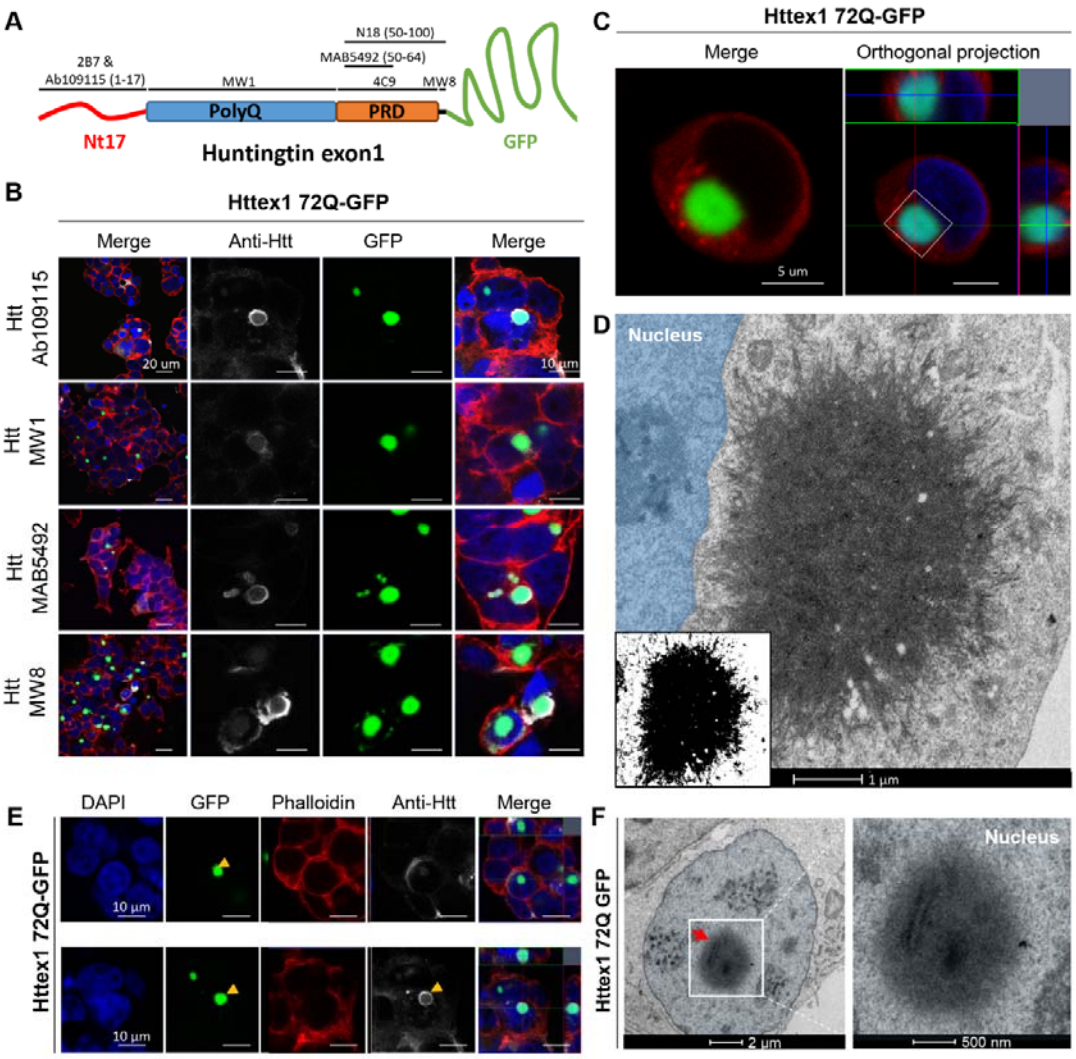

Figure 7. The addition of GFP to the C-terminal part of Httex1 induces a differential structural organization as revealed by ICC and CLEM. A. Epitope mapping of the Httex1 antibodies. **B.** Httex1 72Q-GFP inclusions formed 48 h after transfection in HEK cells were detected by ICC staining combined with confocal imaging. All Htt antibodies showed strong immunoreactivity to the periphery of the Httex1 inclusions and modest immunoreactivity to the core. The nucleus was counterstained with DAPI (blue) and the F-actin with phalloidin (red). Scale bar = 20 µm (left-hand panels) and 10 µm (middle and right-hand panels). **C-D.** 48 h post-transfection, HEK cells were fixed, and ICC against Httex1 was performed and imaged by confocal microscopy (**C**). Scale bars = 5 µm. The selected area of the cells (white square) was then examined by EM (**D**). A binary image (inset) was generated from the electron micrograph using a median filtering and Otsu intensity threshold, allowing for a better distinction of the inclusions' morphology. Scale bar = 500 nm. **E.** Representative confocal images of Httex1 72Q-GFP nuclear inclusions formed in HEK cells 48 h after transfection. Httex1 expression (grey) was detected using a specific antibody against the N-terminal part of Htt (amino acids 1-17; 2B7 or Ab109115), and GFP (green) directly visualized in the appropriate channel. The nucleus was counterstained with DAPI (blue), and phalloidin (red) was used to stain filamentous actin. Httex1 nuclear inclusions are indicated by yellow arrowheads. Scale bars = 10 µm. **F.** Electron micrograph of a representative Httex1 72Q-GFP inclusion. The white square indicates the area shown at higher magnification in the right-hand panel. The nucleus is highlighted in blue. Scale bar = 2 µm (left-hand panel) and 500 nm (right-hand panel).

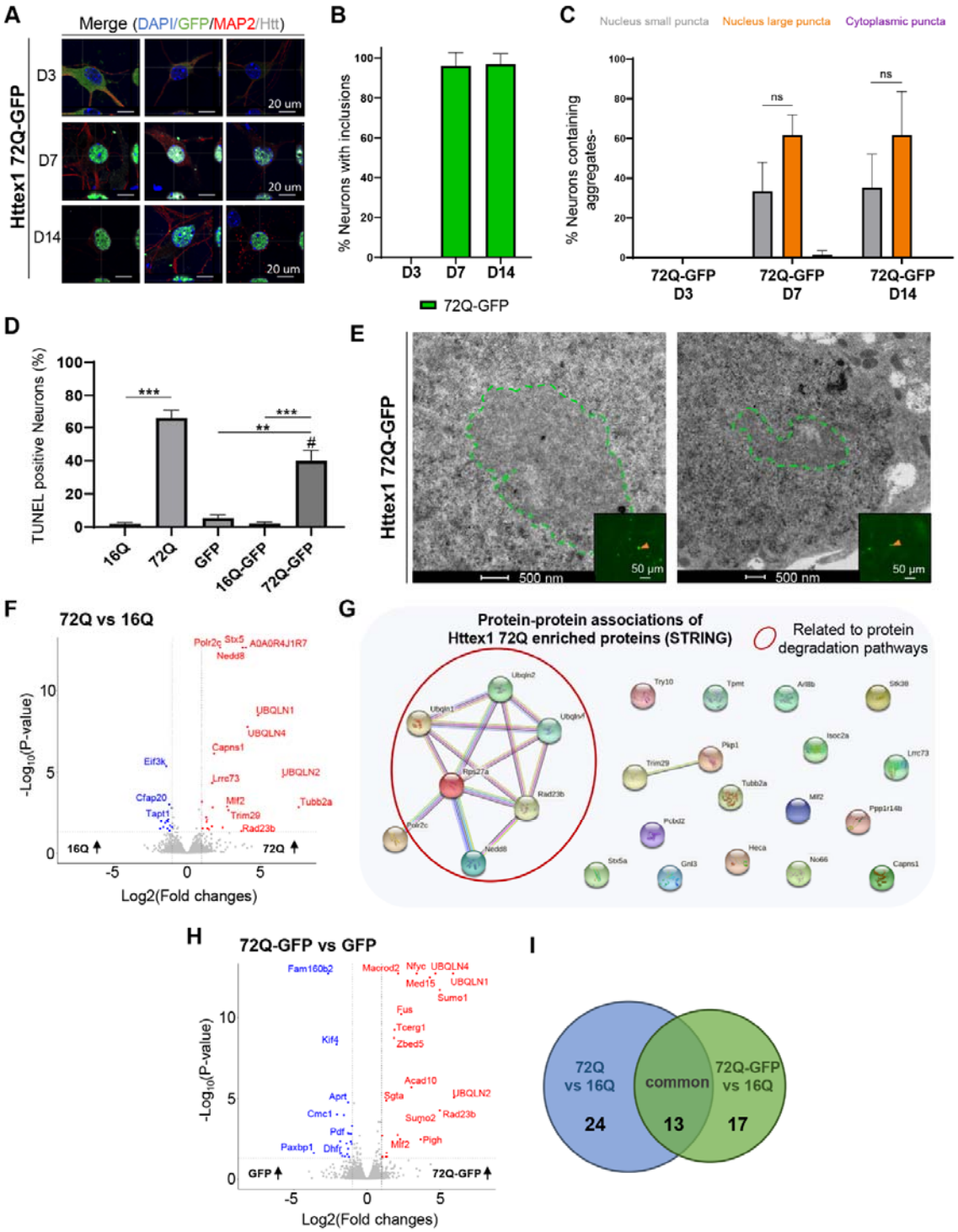

Figure 8. The presence of the GFP tag alters the kinetic, ultrastructural properties, protein content and toxicity of Httex1 72Q inclusions in primary neurons. A. Httex1 72Q-GFP expression was detected by ICC staining combined with confocal imaging in primary cortical neurons, 3- (D3), 7- (D7) and 14- (D14) days after lentiviral transduction. Httex1 was directly visualized with GFP (green) as diffuse, small puncta or large inclusions. The nucleus was counterstained with DAPI (blue), and MAP2 was used to detect the neurons (red). Scale bar = 20 µm. **B.** Image-based quantification of the number of transduced neurons bearing Httex1 72Q-GFP inclusions over time. The graphs represent the

mean ± SD of 3 independent experiments. ANOVA followed by a Tukey honest significant difference [HSD] post hoc test was performed. *P < 0.05, **P < 0.005, ***P < 0.001. **C.** The image-based pipeline Figure 5C was used to classify the morphology (small nuclear puncta *vs.* large nuclear inclusion), and subcellular localization (cytosol *vs.* nucleus) of the inclusions formed upon overexpression of Httex1 72Q-GFP in neurons overtime **D.** TUNEL (Terminal dUTP Nick End-Labeling) assay showed an increased level of DNA fragmentation ($TUNEL^+$) in the neuronal population (positive for the neuronal marker NeuN+) in conditions of overexpression of Httex1 72Q and Httex1 72Q-GFP but not Httex1 16Q, Httex1 16Q-GFP or GFP alone. The graphs represent the mean ± SD of 3 independent experiments. ANOVA followed by a Tukey honest significant difference [HSD] post hoc test was performed. *P < 0.05, **P < 0.005, ***P < 0.001. #P < 0.05 comparison between 72Q and 72Q-GFP. **E.** Representative electron micrographs of Httex1 72Q-GFP inclusions formed after 7 days post lentiviral transduction in mouse cortical primary neurons. Green dashed lines represent the inclusions. Scale bars = 500 nm for the EM images and scale bars = 50 µm for the fluorescent image (inset). **F.** Urea soluble proteins from primary neurons expressing Httex1 72Q or Httex1 16Q of 3 independent experiments were extracted 7 days after lentiviral transduction and analyzed using LC-MS/MS. Identified proteins were plotted using a volcano plot comparing Httex1 72Q vs. Httex1 16Q. Black dotted lines represent the false discovery rate (FDR) <0.05, and an absolute log2 fold change threshold of 1 which were used for assigning significance for the subsequent analysis. 23 proteins upregulated are in red, and the14 downregulated are in blue. The non-significant proteins are in grey. **G.** Visualization of the upregulated Httex1 72Q proteins compared to Httex1 16Q and protein-protein associations using the online platform STRING underscores an association between proteins related to protein degradation pathways (red circle). **H.** Urea soluble proteins from primary neurons expressing Httex1 72Q-GFP or GFP of 3 independent experiments were extracted 7 days after lentiviral transduction and analyzed using LC-MS/MS. Identified proteins were plotted using a volcano plot comparing Httex1 72Q-GFP *vs*. GFP. Black dotted lines represent the false discovery rate (FDR) <0.05 and an absolute log2 fold change threshold of 1 which were used for assigning significance for the subsequent analysis. Upregulated proteins for Httex1 72Q-GFP are represented in red, downregulated in blue and non-significant proteins in grey. **I.** Venn diagram comparison of proteins enriched in Httex1 72Q *vs.* Httex1 16Q (blue) to Httex1 72Q-GFP *vs.* Httex1 16Q (green). 24 proteins were unique to Httex1 72Q *vs.* Httex1 16Q (44.4%), 17 unique to Httex1 72Q-GFP *vs.* Httex1 16Q (31.5%) and 13 (24.1%) common to both co-aggregated proteins.

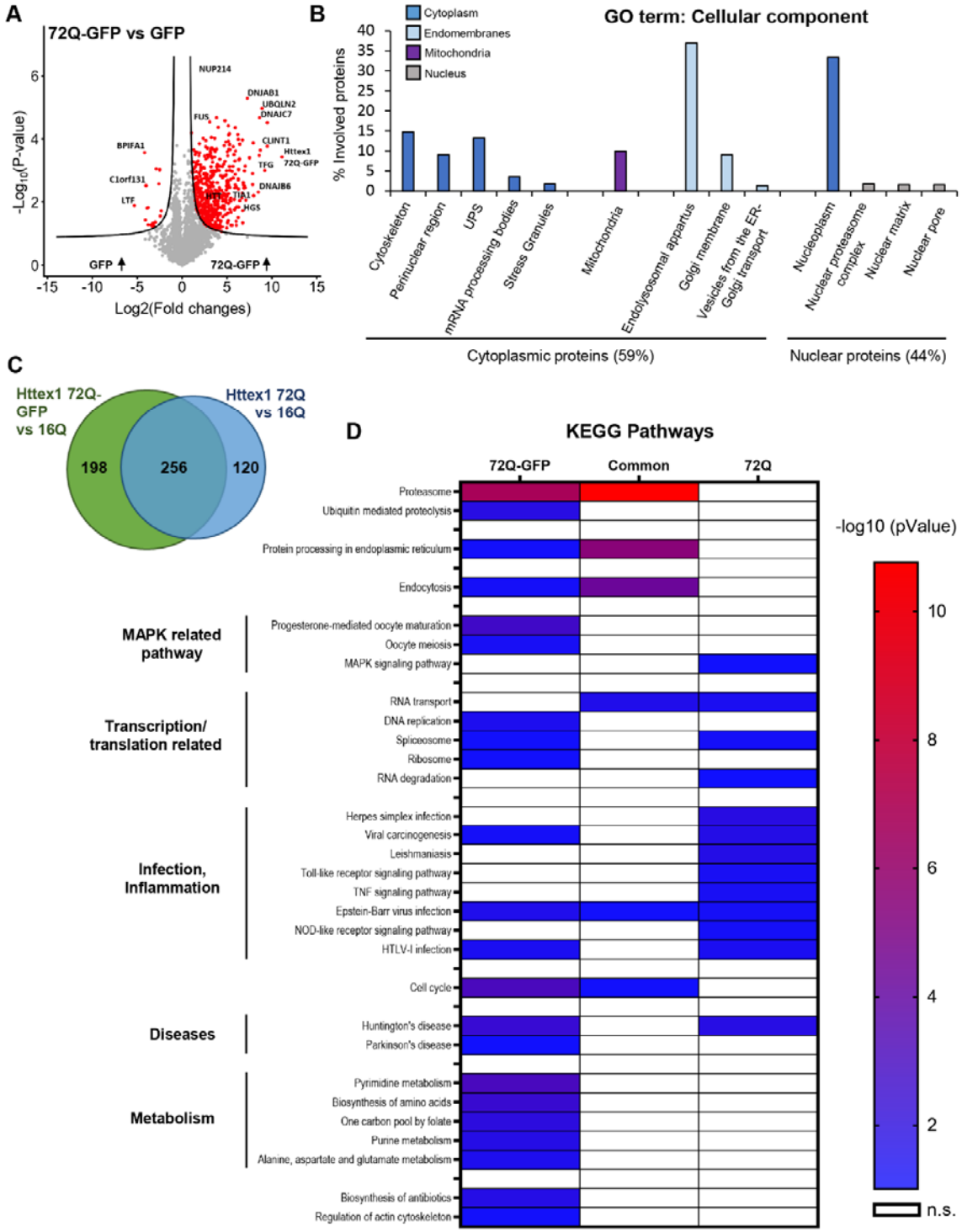

Figure 9. Proteomic analysis of Httex1 72Q-GFP in the Urea soluble fraction revealed 55% differences compared to tag-free Httex1 72Q for the proteins co-aggregated with Httex1 in HEK cells. A. Identified proteins were illustrated using a volcano plot for the comparison of protein levels identified in the Urea soluble fraction 48 h after Httex1 72Q-GFP or GFP transfection in HEK cells, in 3 independent experiments. Mean difference (Log2 (Fold-Change) on the X-axis) between the Urea soluble fraction of HEK cells overexpressing Httex1 72Q-GFP or GFP were plotted against significance (Log10 (p-Value) on the Y-axis (T-Test)). A false discovery rate (FDR) of 0.05 and a threshold of significance S0=0.5 were

assigned for the subsequent analyses. **B.** Cell compartment classification of the proteins significantly enriched in the Urea soluble fraction of the HEK cells overexpressing Httex1 72Q-GFP versus those expressing GFP. Gene Ontology (GO) enrichment analyses were determined by DAVID analysis (p values<0.05). **C.** To compare the results obtained with Httex1 72Q-GFP to tag-free Httex1 72Q, we represented the proteins enriched in Httex1 72Q vs. Httex1 16Q compared to the proteins enriched in Httex1 72Q-GFP vs. Httex1 16Q using a Venn diagram. In total, 256 proteins (44.6%) were found similar between the two conditions, 198 proteins (34.5%) were unique for Httex1 72-GFP enrichment, and 120 proteins (20.9%) were for Httex1 72Q enrichment. **D**. Kyoto Encyclopedia of Genes and Genomes (KEGG) Pathway Analysis of co-aggregated proteins with Httex1 72Q and Httex1 72Q-GFP. The heat map represents significant pathways (KEGG) enriched in the Urea soluble fractions extracted from the Venn diagram (**C**): co-aggregated proteins unique to Httex1 72Q, unique to Httex1-72Q-GFP, and common to both conditions, all compared to Httex1 16Q control.

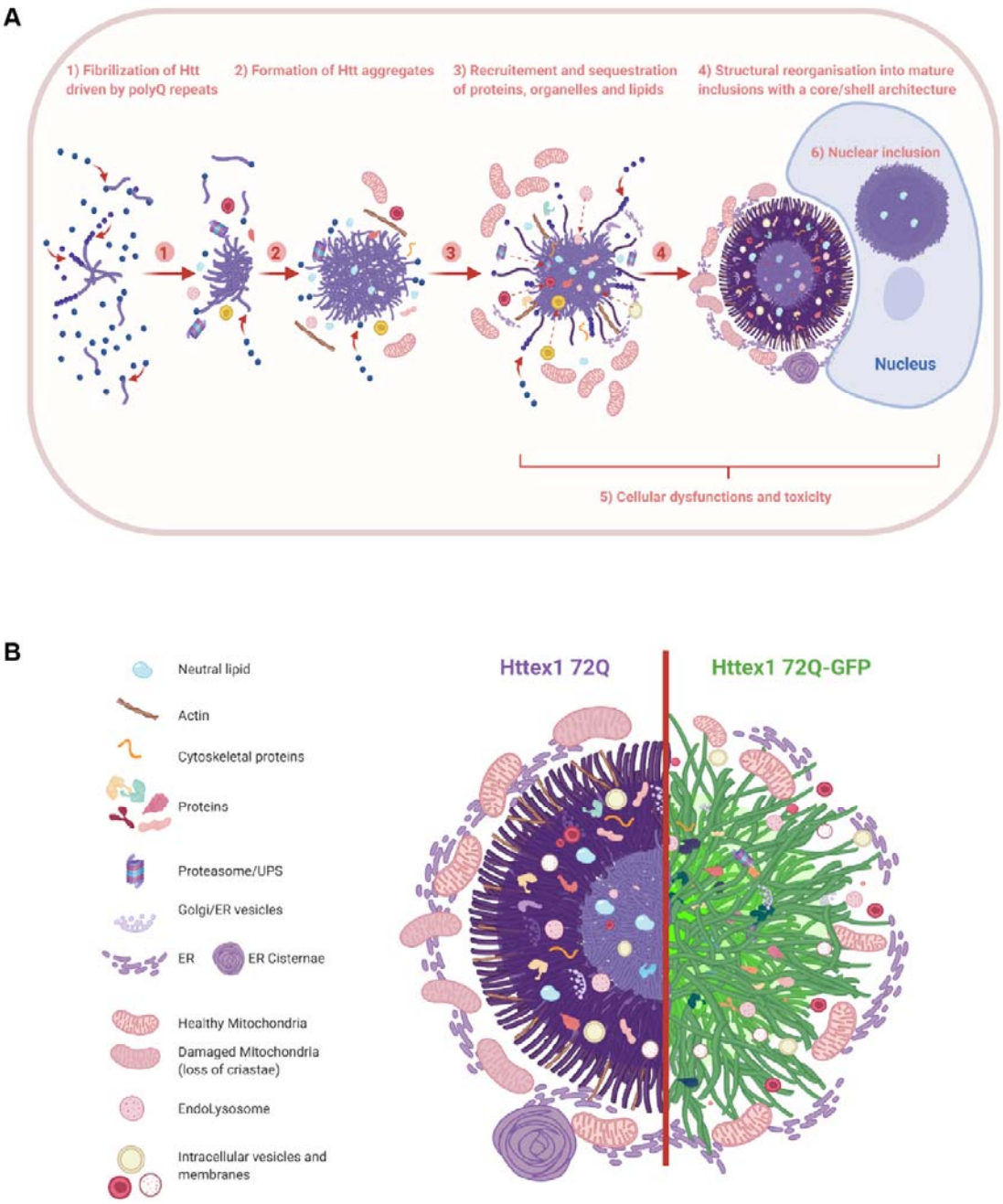

Figure 10. The formation of Huntingtin inclusions is driven primarily by the polyQ repeat domain and involves the active recruitment and sequestration of lipids, proteins, and membranous organelles. A. We separated the formation and organization of cytoplasmic Httex1 inclusions in different elements: 1) Even though the Nt17 domain can play a major role in early oligomerization steps, we showed that the fibrilization is driven by the polyQ repeats; 2) The initiation of inclusion formation was previously demonstrated to occur in a phase transition mechanism[14,31] and could involve first the sequestration of proteins and organelles nearby either directly or indirectly; 3) During the growth of the inclusion, many cellular proteins, endomembranes, and lipids are recruited and sequestered inside the cytoplasmic inclusions; 4) Mature cytoplasmic Httex1 inclusions formed in cells display a core and shell structural organization if the polyQ length is relatively long (72Q) but

not if it is close to the pathogenic threshold (39Q), even if inclusions are still formed in the second case. Cytoplasmic inclusion formation leads to the accumulation of mitochondria and ER network at the periphery; 5) Httex1 inclusion formation leads to the adaptation of the ER-mitochondrial network and respirational dysfunction, as well as significant toxicity after long-term incubation; 6) Nuclear inclusions do not display a distinct core/shell organization similar to the cytoplasmic inclusions, but they are still detected as a ring, as they are impervious for antibodies. Nuclear tag-free Httex1 inclusions are also enriched in neutral lipids. **B.** The depiction shows the distinct structural organization and cellular impact of Httex1 72Q (left) compared to Httex1 72Q-GFP (right). The arrangement and packing of Httex1 fibrils are different depending on the presence of GFP as well as the interactions, recruitment, and perturbation with surrounding organelles.